CLM - P 518

CLM - P 518

UKAEA

Preprint

POST ACCIDENT HEAT REMOVAL

R S PECKOVER

CULHAM LABORATORY
Abingdon Oxfordshire

1978

CLM-P 518

POST ACCIDENT HEAT REMOVAL

R S Peckover

UK Atomic Energy Authority
Culham Laboratory, Abingdon, U.K.

ABSTRACT

In the unlikely event of the meltdown of a nuclear reactor core, the primary concern is to keep the radioactive fission products within some containment skin. This implies that molten core debris must be prevented from melting its way out of the containment, if necessary by specifically designed containment barriers. Fundamental knowledge of heat transfer and fluid mechanics of internally heated systems is required and this paper reviews published material on the broad background areas of information which are needed in assessing such devices.

Paper presented at the meeting on "Thermohydraulic Problems related to Reactor Safety", Euratom Joint Research Centre, Ispra, September 1977.

October 1977

I. INTRODUCTION

In the unlikely event of the meltdown of a nuclear reactor core, the primary concern is to keep the radioactive fission products within some containment skin. Containment might be breached either by high pressures or high temperatures. We shall be concerned here with methods of preventing molten core debris from melting its way out of the containment. Devices to achieve this are called 'core catchers' and may be within the primary vessel, or ex-vessel.

In section 2 we shall consider briefly possible ways in which a meltdown could develop. As will be clear when we examine in section 8 possible forms of catcher device, fundamental knowledge of heat transfer and fluid mechanics of internally heated systems is required in assessing all such devices. The aim of this paper is to review the broad background areas of information which are needed.

Post Accident Heat Removal (PAHR) studies are still developing. Reference is given in the reference list to recent conferences where significant papers on core debris control have been presented. [1-5].

II. ACCIDENT SEQUENCE AFTER CORE MELTDOWN

Once at least part of the core is molten, its location is no longer fixed in space and its subsequent behaviour may be rather complicated. The aim must be to ensure that the core debris reaches a site where it can be cooled and hence resolidified without the release of radioactive fission products to the environment. The core debris may be in several different forms. In a gas cooled fast reactor, after melting, the core support structure will slump (in the absence of adequate cooling) and a mixture of fuel, fuel cans, and support structure can form in the bottom of the vessel as an amorphous heap. In time the decay heat is likely to transform this into a molten pool. In a sodium cooled fast reactor however UO_2 may fragment on contact with liquid sodium resulting in the core debris being in the form of particles in the 100 micron range. Fig. 2.1,[26], gives a flow chart of events for PAHR analysis.

From this, one can see that knowledge of the magnitude of decay heat to be removed, and of the behaviour of particulate beds, molten pools and advancing melting fronts is of basic importance. Additional complications arise because of the possibility of recriticality, and the presence of concrete. A detailed analysis of accident sequences is only possible for a particular reactor design, and is inappropriate here.

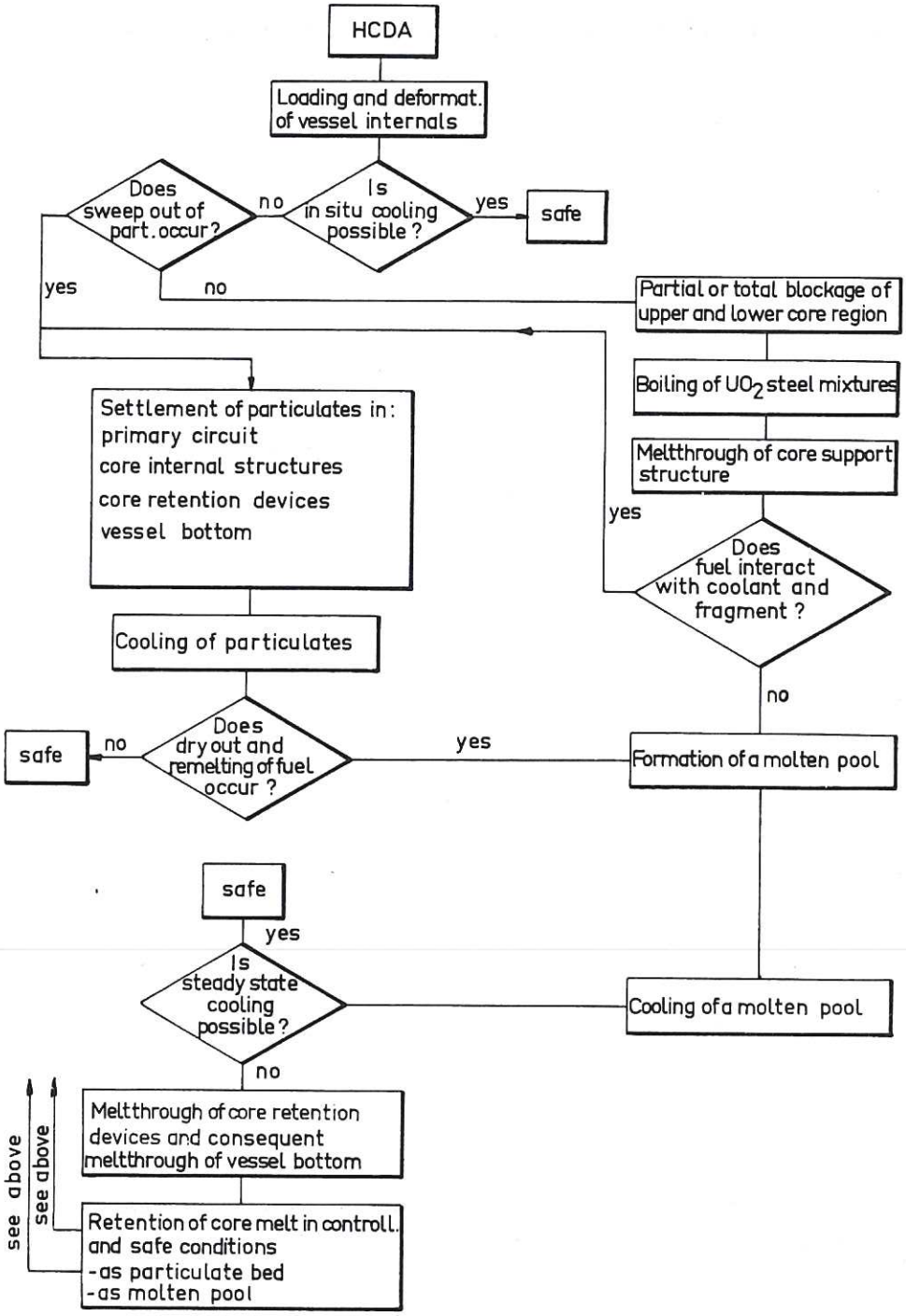

Fig. 2.1 Flow Chart of Events for PAHR Analysis [56]

III. FISSION PRODUCT DECAY HEAT

After a nuclear reactor has been shut down, having been on power, it continues to generate heat. This heat arises from the continued presence of neutrons that cause further fissions and from the emission of beta particles and gamma rays by the radioactive decay of the various fission products. The first mechanism is much less important than the second and is usually evident only in the first few moments after shutdown.

The energy released in fission-product decay heat depends upon the beta- and gamma-ray energies of the decay steps in all the decay chains, together with their half-lives and relative abundance in the core. The power generation P due to beta and gamma rays can be expressed as a fraction of the reactor power before shutdown P_o in the following form

$$P/P_o = f(t) - f(t + T_o)$$

where t is the time since shutdown and T_o is the period of reactor operation prior to shutdown. Way and Wigner made the first definitive estimate of the decay heat function: it is $f_{ww} = 6.22 \times 10^{-2} t^{-0.2}$. This gives results good to $\sim$ a factor of two for 10 sec < t < 100 days. The American standard decay heat function for light water reactors is based on the work of Shure, it has the form $f_{ANS} = At^{-a}$ where the constants A and a are assigned different values in different intervals as in table 3.1 below.

A realistic upper limit to the decay heat is required for decay studies. No data set for fast reactors is as well established as the ANS standard for thermal reactors; a conservative approach is to use the ANS standard for the fission product contribution for a fast reactor, and then to make allowances for the other contributions e.g. the decay heat from the actinides by a safety factor of up to 50%. Figure 3.1 shows the ANS curve for irradiation time of 10^8 secs, and a decay heat curve for a fast reactor based on the Way-Wigner formula.

Applicable Time Interval (sec)	A	a
$10^{-1} \leq t < 10^{1}$	12.05	0.0639
$10^{1} \leq t \leq 1.5 \times 10^{2}$	15.31	0.1807
$1.5 \times 10^{2} < t < 4 \times 10^{6}$	26.02	0.2834
$4 \times 10^{6} \leq t \leq 2 \times 10^{8}$	53.18	0.3350

Table 3.1 Constants for ANS decay curve [8]

Of the fission products which are not volatile below 3000°C, some have stable oxides which remain in the mixed oxide fuel and some such as molybdenum and ruthenium migrate into the molten iron debris to form a metallic alloy. [Fischer et al (1973)]. The presence of two distinct phases, oxide and alloy, each containing some heat generating fission products, may complicate the modelling.

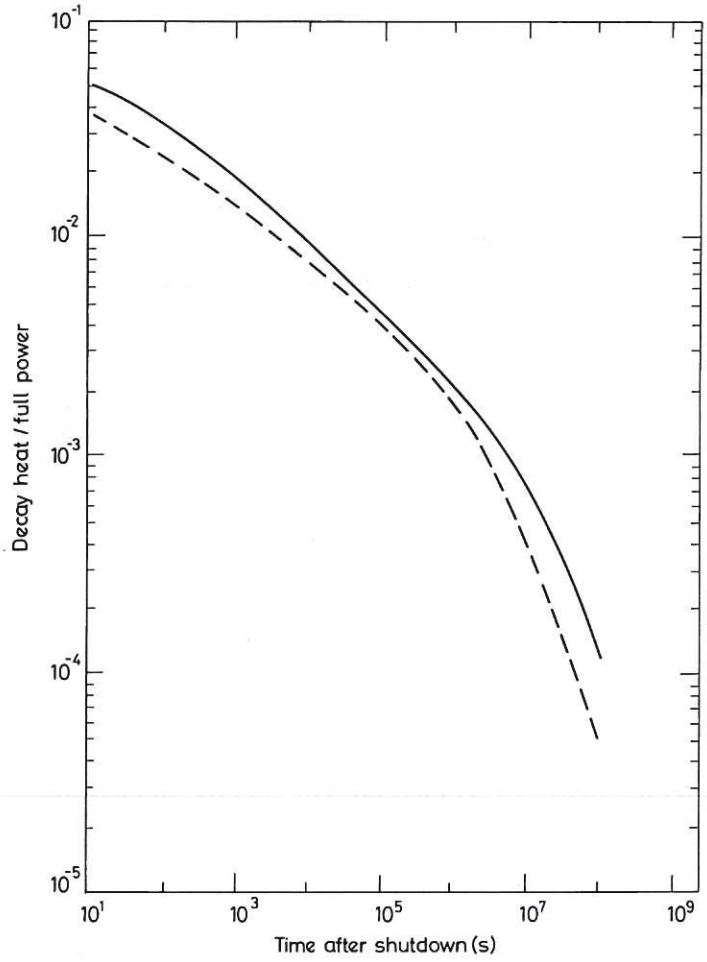

Fig. 3.1

Decay heat curves: contribution from fission products

——— ANS standard for irradiation time of 10^8 sec.

- - - Way-Wigner formula for PFR conditions.

IV. MOLTEN POOLS

Core debris may form into molten pools after the dry out of particulate beds, or from the overheating of solid lumps. In section IV.1 we consider shallow pools

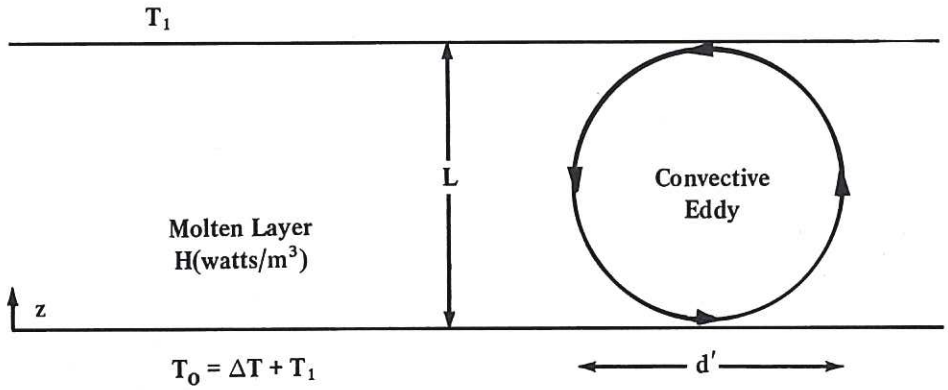

Fig. 4.1 Internally heated convecting molten layer with applied temperature gradient

of infinite horizontal extents - horizontal layers; in section IV.2 finite aspect ratio pools are considered; in section IV.3 boiling is discussed.

IV.1 Molten Layers

Consider a molten layer as shown in fig. 4.1 which is of depth L with a uniform volumetric heat source H (watts/m^3). Let the upper surface be at a temperature T_1 and the lower surface at T_o. Let z be the vertical co-ordinate measured upwards from the bottom surface. Then, in the absence of convection, the temperature satisfies the thermal conduction equation

$$k \frac{\partial^2 T}{\partial z^2} + H = 0$$

which has as its solution

$$T_o - T = (T_o - T_1)(\frac{z}{L}) - T_H(\frac{z}{L}) \cdot (1 - \frac{z}{L})$$

where $T_H = HL^2/2k$. If $T_H = 0$ then only an applied temperature difference $(T_o - T_1)$ remains, which if positive, and sufficiently large results in Benard convection (see §IV.1.1). If $T_o = T_1$, only internal heating is present - the classical Kulacki-Goldstein configuration. The ratio $S \equiv (T_o - T_1)/T_H$ is an important parameter in what follows; it is a measure of strength of external to internal energy sources, and is in fact the ratio of Rayleigh numbers Ra/Ra_H (defined in the following sections). The criteria for the onset of convection of such a system have been established by Sparrow, Goldstein and Jonsson (1964). Other detailed discussions are by Kulacki (1971), Joseph (1976) and Gershuni and Zhukhovitsky (1976).

In the following sections, the Benard problem is discussed first, as it is the most familiar, then the internally heated layer with adiabatic bottom, then the internally heated layer with equal and finally unequal temperatures. As will emerge this forms a logical progression through the results of heat transfer in molten layers.

IV.1.1 Benard Convection Here a temperature difference $\Delta T \equiv T_o - T_1$ is imposed across the layer. From simple arguments that lighter fluids will rise in an environment of heavier material, one would expect convection to occur whenever $\Delta T > 0$. In practice the fluid has a kinematic viscosity ν which impedes movement of a blob, and a thermometric conductivity κ which reduces the temperature difference between the blob and its surrounding. Hence persistent convection does not set in until ΔT exceeds a critical ΔT_c. A non-dimensional form of the temperature difference, called the Rayleigh number Ra, is defined by

$$Ra = \alpha g \Delta T L^3/\nu\kappa$$

Convection occurs when $Ra > Ra_{crit}$ where R_{crit} is $\sim$ 1708 when the surfaces are rigid plates, $\sim$ 1100 when the upper surface is free and the lower rigid, and $\sim$ 657 (exactly $\frac{27}{4}\pi^4$) when both surfaces are free. Although this last case is normally only achievable in stellar atmospheres, it has been used as the basis for many analytical and numerical studies because it is mathematically tractable. In plan form steady laminar convection may occur in the form of rolls, squares or hexagons, but in all cases the horizontal length scale d' is such that (d'/L) is of order unity. For convection to begin the depth of a layer is quite small as table 4.1 indicates.

layer depth	water	air	steel
1 cm	4.29	9.03	40.9
10 cm	.004	.009	.040

Table 4.1 ΔT_{crit} for the onset of convection between rigid plates

For $1 < R^* \lesssim 100$ (where $R^* = Ra/Ra_{crit}$) convection is laminar and has a marked cellular structure. The regions of down flow or up flow become increasingly narrow and a core region develops in which the temperature is roughly constant at $T_o + \frac{1}{2}\Delta T$. The flow pattern can be considered as composed of two boundary layers within which the heat transfer process is concentrated. The vertical transfer in the plume part is essentially by convection. Within the horizontal boundary layers heat is transferred by conduction to and from the moving streams of fluid.

When the velocity in the boundary layers becomes high enough, the steady flow patterns breakdown in a series of transitions and the flow becomes turbulent. At high Rayleigh numbers the layer consists of two thin boundary layers, one on each horizontal plate, separated by a turbulent region which is essentially isothermal. Within the boundary layers the heat transfer to the plates is by conduction. Within the turbulent region heat transfer is turbulent, but it is difficult to characterize this by a simple turbulent eddy heat transfer coefficient since the mean temperature gradient is essentially zero.

The Nusselt number Nu is defined as

$$Nu = \frac{\psi L}{k\Delta T}$$

where k is the thermal conductivity and ψ is the thermal flux carried from one plate to another. It can be thought of as a non-dimensional effective thermal

conductivity: $Nu = k_{effective}/k$.

When the boundary layers are very thin it seems plausible that the heat transfer rate is independent of the thickness of the turbulent region separating them. If one assumes that $Nu \propto Ra^n$ for some exponent n, then $Nu \propto Ra^{1/3}$ and $\psi \propto (\Delta T)^{4/3}$. In fact even for quite deep layers the overall layer depth still has some small effect for many experiments in air and water are quite unanimous that $n < \frac{1}{3}$.

Typical experimental results are given in the table below for the constants a,b in the correlation $Nu^* = a(Ra)^b$ where $Nu^* = Nu/Nu_{cond}$ and Nu_{cond} is the value of the Nusselt number in the absence of convection. For Benard convection $Nu_{cond} = 1$.

Table 4.2. Benard Convection Experiments

Author	Fluid	a	b	range
Fitzjarrald	air	0.130	0.30	$4 \times 10^4 < Ra < 7 \times 10^9$
Garon & Goldstein	water	0.130	0.293	$1.3 \times 10^7 < Ra < 3.3 \times 10^9$
Chu & Goldstein	water	0.183	0.278	$2.76 \times 10^5 < Ra < 1.05 \times 10^8$

Dearsdorff (1970) has shown that a key quantity in turbulent thermal convection is the dimensionless group $\Lambda \equiv Pr.Ra.Nu \equiv \alpha g \psi L^4/(k\kappa^2)$ where Pr is the Prandtl number. The viscosity dependence in this modified Rayleigh number is eliminated as one would expect once turbulence is well established. The characteristic convective velocity $\omega^* = \frac{\kappa}{L} \Lambda^{1/3}$ and a characteristic temperature fluctuation is $T^* = \Delta T \, Nu \, \Lambda^{-1/3}$ so that $\psi = \rho c \omega^* T^*$ (where ρ and c are the density and specific heat of the fluid).

IV.1.2 Internally Heated Convection: Adiabatic Bottom

Next we consider a horizontal layer heating internally by a uniform volumetric heat source, and with an adiabatic lower surface. Such a situation could be approximated by for example, molten steel containing metallic heat-producing fission products lying over a thick layer of solid depleted UO_2. All of the heat generated in the layer is transported to the top surface which is maintained at some cool temperature. At sufficiently high heat generation rates turbulent convection will occur, and the bulk of the fluid will have a constant mean temperature, with a thin boundary layer above it adjacent to the isothermal top boundary. It is found experimentally that $Nu^* = a_1 (Ra_H)^{b_1}$ where Ra_H is the internal heat generation rate based on

Rayleigh number $\alpha g H L^5/(2k\kappa\nu)$ where H is the uniform rate of heat generation (in watts/cc). The table gives typical experimental results. For this configuration $Nu_{cond} = 2$. [warning: it is important when comparing papers on thermal convection to pay attention to the precise definitions used for Nu, Ra etc.]. The quantity $HL^2/2k \equiv T_H$ is the temperature difference across the layer in the absence of convection.

Table 4.3 Internally heated convection experiments in adiabatic bottom

authors	fluid	a_1	b_1	range
Fiedler & Wille	water	0.262	0.228	$2 \times 10^5 < Ra_H < 6 \times 10^8$
Ralph & Roberts	water	0.192	0.244	$5 \times 10^4 < Ra_H < 4 \times 10^{10}$
Kulacki & Nagle	water	0.1525	0.239	$1.5 \times 10^5 < Ra_H < 2.6 \times 10^9$
Kulacki & Emara	water	0.2015	0.226	$1.1 \times 10^4 < Ra_H < 2.1 \times 10^{12}$

It is possible to derive the (Nu^*-Ra_H) relationship above from the (Nu^*-Ra) relationship for turbulent Benard convection. In both cases the bulk of the fluid is essentially at a constant temperature. In Benard convection, the thermal flux through the cell is independent of the vertical co-ordinate z, whereas in internally heated convection, the flux increases linearly. However one can argue that in the upper boundary layer, of thickness $\sim L/2Nu^*$, the relationship between overall flux and the overall temperature difference should be identical. For Benard convection $\psi \propto (\Delta T)^{1+b}$; for internally heated convection $\psi^{(1-b_1)} \propto \Delta T$. Hence $b_1 = b/(1+b)$. Similarly, when the correct temperature difference is used, $a_1^{1+b} = a$. If we use the Garon-Goldstein correlation, since it is restricted to the higher ranges of Ra, then $b = 0.293$, $a = 0.130$, from which one can derive $b_1 = 0.227$ $a_1 = 0.190$. The agreement between this prediction and the experimental results of Kulacki and Emara is striking.

Fig. 4.2
Vertical Temperature Profile for different values of R* [44]

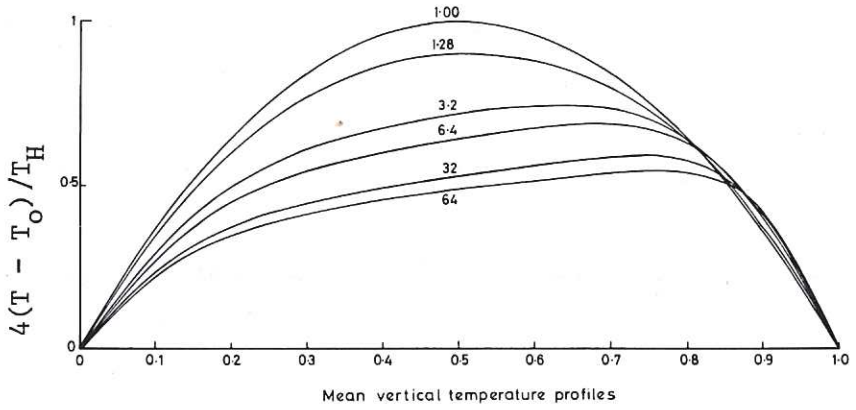

IV.1.3 Internally Heated Convection: Equal Isothermal Surfaces. In a horizontal layer heated uniformly by a volumetric heat source, and with top and bottom surfaces maintained at constant and equal temperatures $T_o = T_1$, the temperature profile in the absence of convection is a symmetric parabola. As the heating rate is increased the temperature profile flattens even though the mean temperature increases. Boundary layers develop on the top and bottom plates; because buoyancy carries heat upwards, the upper boundary layer is much thinner than the lower one and a larger fraction of the heat generated is expelled through the upper surface than the lower one [see fig. 4.2]. The fluxes ψ_1 and ψ_o through the upper and lower surfaces can be expressed in terms of Nusselt numbers Nu_1 and Nu_o to which there corresponds $Nu_1{}^*$ and $Nu_o{}^*$, as above. For this configuration $Nu_{cond} = 4$. Experimental results are given in the table 4.4 for the constants a_3, b_3, a_4, b_4 in

$$Nu_1{}^* = a_3(Ra_H)^{b_3}$$
$$Nu_o{}^* = a_4(Ra_H)^{b_4}$$

Table 4.4 Internally heated convection experiments: $T_o = T_1$

authors	fluid	a_3	b_3	a_4	b_4	range of Ra_H
Kulacki & Goldstein	water	0.097	0.236	0.381	0.094	$2 \times 10^4 - 1.2 \times 10^7$
Jahn & Reineke	water	0.101	0.233	0.371	0.095	$5 \times 10^5 - 5 \times 10^8$
Ralph et al	water	0.062	0.238	0.072	0.175	$2.10^8 - 5 \times 10^{11}$

A convenient way of considering the heat transfer from a layer heated volumetrically is to divide it into 2 sublayers, the ratio of whose depths are proportional to the respective fluxes (Peckover 1972). When this is done, the lower layer is essentially a conduction layer in which all the heat generated in it is conducted downwards. The experimental profiles are consistent with this, and the Nusselt number based on this layer depth remains close to 2 - the conduction value. The upper layer is convection controlled. Baker, Faw and Kulacki (1976) have calculated the sublayer Nusselt numbers from the Kulacki-Goldstein data (see fig. 4.3). When the Rayleigh number Ra_H is modified to be that for the upper sublayer $Ra_H^u = (L_1/L)^5 Ra_H$, there is satisfactory agreement between the correlation $Nu_1' - Ra_H^u$ and that for internally heated convection with an adiabatic bottom. (see fig. 4.4). The plane separating the two sublayers thus has, to a first approximation, zero net heat transfer; the fact that the hydrodynamic boundary condition differs from the rigid one of section IV.1.2 is apparently unimportant.

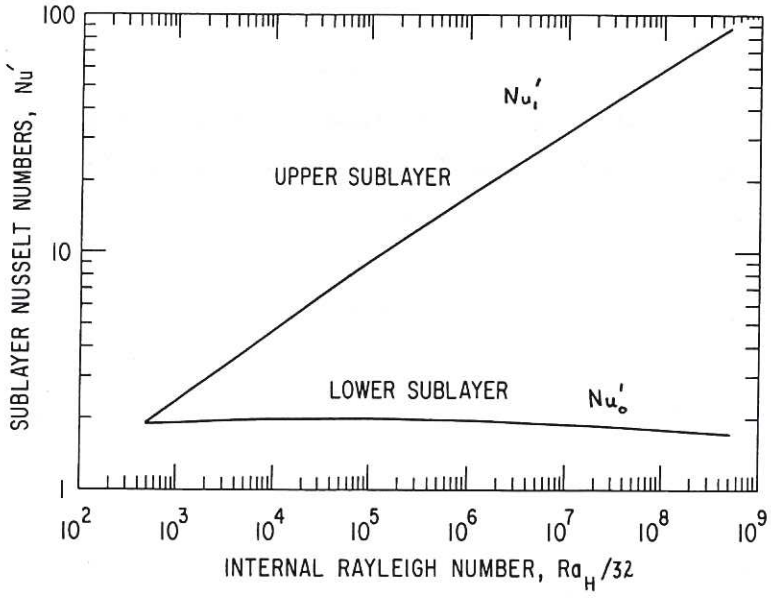

Fig. 4.3 [9]
Nusselt numbers based on the appropriate sublayer depth vs Internal Rayleigh Number Ra_H

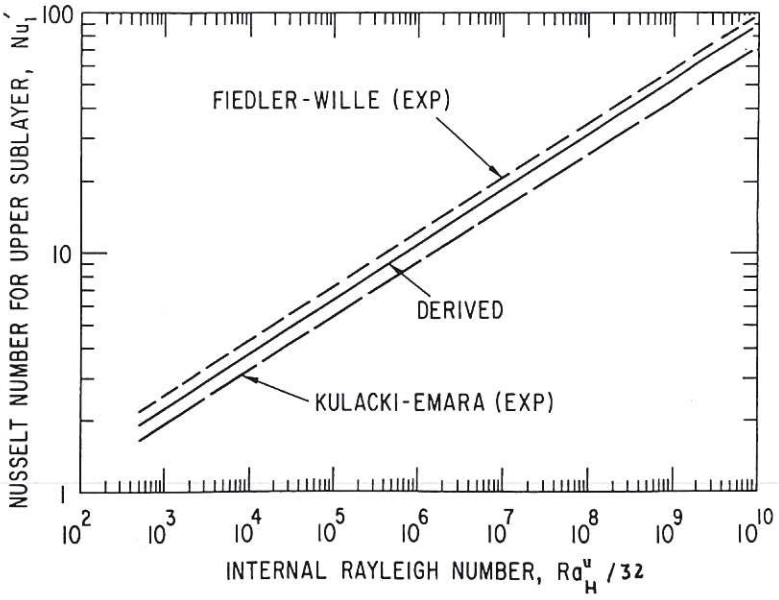

Fig. 4.4 [9]
Comparison between Nusselt number for upper sublayer for $T_o = T_1$ boundaries with that for adiabatic bottom

IV.1.4 Internal Heat Convection: Unequal Isothermal Surfaces. If the upper and lower surfaces are maintained at different temperatures while internal heating is also present, then both the ordinary Rayleigh number Ra and that based on internal heating Ra_H are needed to characterize the convection. If the upper surface is at a higher temperature than the lower, then Ra is negative. Baker et al (1977) have extended the two sublayer concept to predict η, the fraction of heat conducted downwards as a function of Ra and Ra_H. Using the Kulacki-Goldstein correlation, (section IV.1.3) coupled with the Kulacki-Emara correlation (section IV.1.2) they obtain the following equation for η

$$(1 - \eta)^{0.870} = \frac{1}{5}(\eta^2 + S)\ (Ra_H)^{0.226} \qquad (4.1)$$

where $S = Ra/Ra_H$. Suo-Antilla and Catton have carried out experiments in this geometry and fig. 4.5 shows a stylized representation of the resulting behaviour.

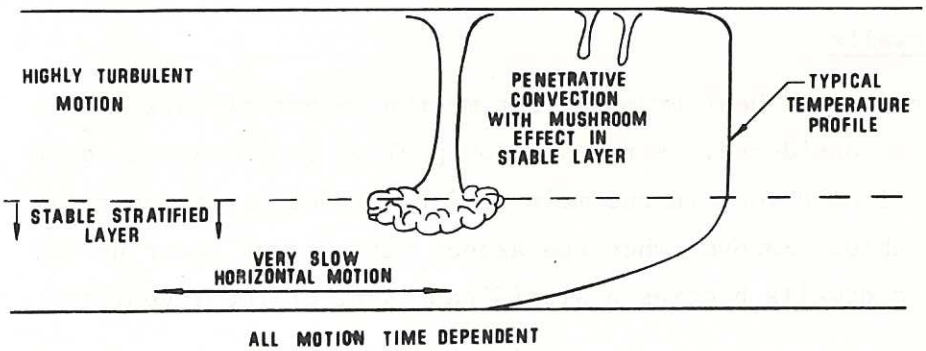

Fig. 4.5 [55] Behaviour in an internally heated layer with unequal top and bottom temperatures

Various regimes may be discerned in fig. 4.6.

(i) if $Ra > 4.97\ Ra_H^{0.774}$, then all the heat is transferred upwards; $\eta = 0$

(ii) if $Ra_H > -Ra > Ra_H\ (1 - [8.25/Ra_H^{1/5}])$, then convection is suppressed and most of the heat is transferred downwards; a small fraction is conducted upwards

(iii) if $-Ra > Ra_H$, all heat is conducted downwards, and there is no convection

(iv) if $|Ra| \ll Ra_H.\eta_o$ then applied temperature differences can be ignored, and the heat fractions are given by η_o and $1 - \eta_o$ respectively. $\eta_o = 1/(1 + \frac{1}{4} Ra_H^{0.142})$ is the value of η when $Ra = 0$.

(v) otherwise equation (4.1) must be used in full.

These equations together constitute, as Baker et al (1976) point out, a complete description for the general case of the non-boiling horizontal fluid layer with uniform internal heat sources, provided the top and bottom surface temperatures are prescribed. For multiple layers, and for convective or radiative boundary conditions, the results are not sufficient to codify in this way.

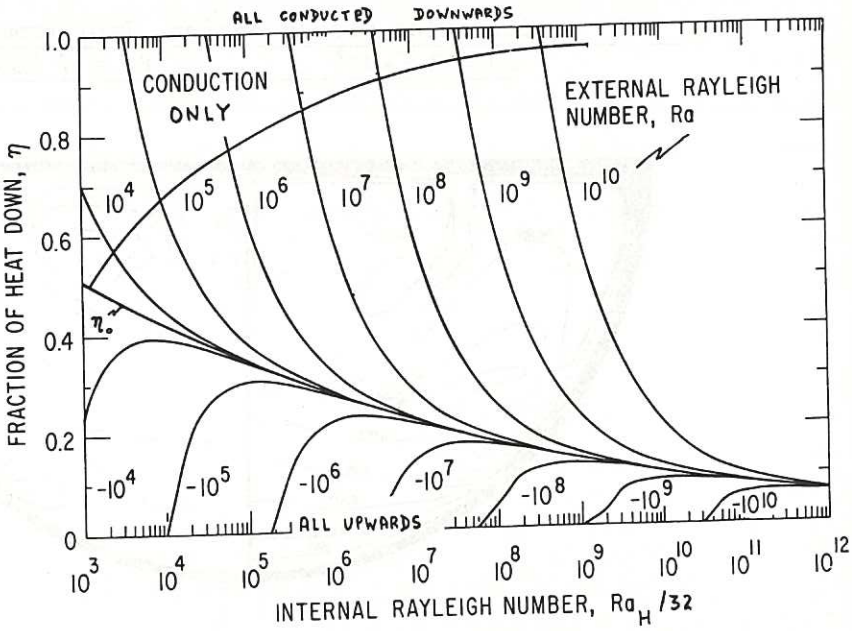

Fig. 4.6 [9] Fraction of heat transferred downwards as a function of Ra and Ra_H

IV.2 Pools with sidewalls

In §IV.1, convection and heat transfer for molten layers of infinite horizontal extent were considered. For a shallow pool of broad extent these correlations will still hold good in the main region - indeed experimentally, sidewalls are unavoidable. However when the aspect ratio is of order unity, heat transfer to the sidewalls becomes a significant part of the inventory.

The lower boundary of a molten pool melting into a sacrificial material takes the form of a trough in 2D or a bowl in 3D. (see §VI). Experiments have been carried out by Jahn and Reineke for internally heated convection in semicircles and hemispheres. In the semicircle the fluid is fairly stagnant at the bottom and the isotherms are roughly horizontal as in a horizontal layer (see fig. 4.7). The heat transfer increases with angle from the vertical until at $\pi/2$ the local Nusselt number is effectively the same as for the horizontal top surface (see fig. 4.8). Essentially the convective flow to the top surface returns down the sidewalls losing heat as it falls. In a hemisphere similar effects are observed, but the radial convergence towards bottom results in the quiescent region being rather small. This results in the ratio of maximum to minimum local Nusselt number being rather smaller for the hemisphere for comparable Rayleigh numbers (fig. 4.9).

These results suggest that for the heat transfer to the side walls they may be considered as cooled plates. For a rectangular geometry this would be a cooled vertical plate in which case the lateral Nusselt number Nu_s is given by $Nu_s = 0.677\ (Pr/\{Pr + 20/21\})^{\frac{1}{4}}\ Ra_{KG}^{\frac{1}{4}}$ where $Ra_{KG} = Ra_H/32$. Experiments by Gabor et al (1975) are in agreement with this formulation.

Fig. 4.7 Semicircular Cross-section. Isotherms and Streamlines
$Ra = 3.5 \times 10^{8}$ $Pr = 7$ [50]

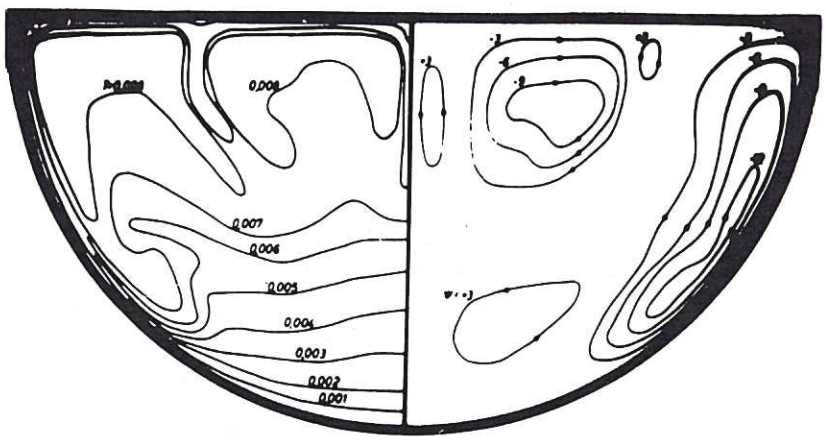

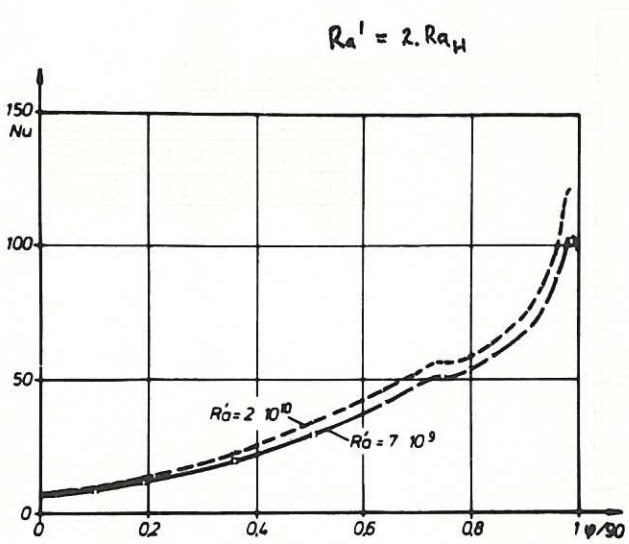

Fig. 4.8 Local Nusselt Number as function of angle: Semi-circular cross-section [50]

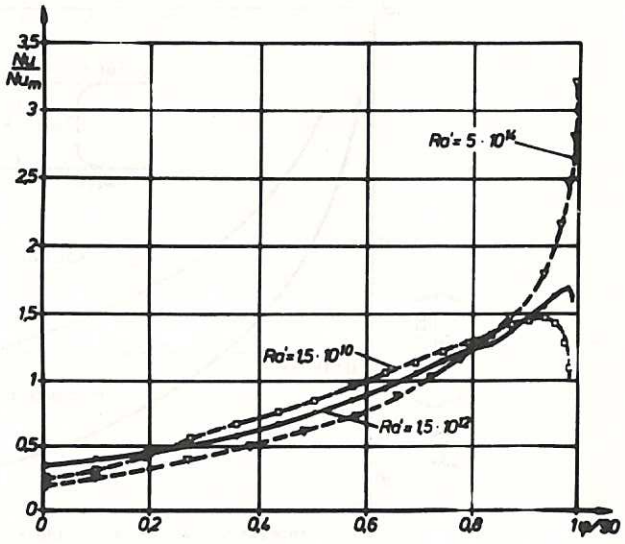

Fig. 4.9 Local Nusselt Number as function of angle: Hemispherical pool [50]

IV.3 Boiling

In a molten layer heated internally, the effect of convection is to flatten the temperature profile. Nevertheless if the heat source density is increased, the maximum temperature also increases though at a slower rate. For equal isothermal surfaces

$$(T_{max} - T_o)\left(\frac{Nu_o + Nu_1}{2}\right) = T_H$$

At a sufficiently high power density H_B the liquid reaches its boiling point. H_B depends on the layer thickness. Fig. 4.10 shows the onset of boiling in UO_2 for the given property values, based on the Kulacki-Goldstein correlations, as calculated by Suo-Anttila et al (1974).

Once boiling occurs the maximum temperature is restricted to be within a few degrees of boiling. Fig. 4.11 [54] shows behaviour in a boiling layer. There is still a quiescent sublayer at the bottom of the layer, and one might expect the downward flux to have the conduction value: $\psi_o = 2\frac{k}{L}\sqrt{T_H(T_{sat} - T_o)}$. In experiments Stein et al (1974) find values up to six times this value. It seems that the boiling process in the main part of the layer induces oscillatory motions in the bottom sublayer which enhances the downward heat transfer.

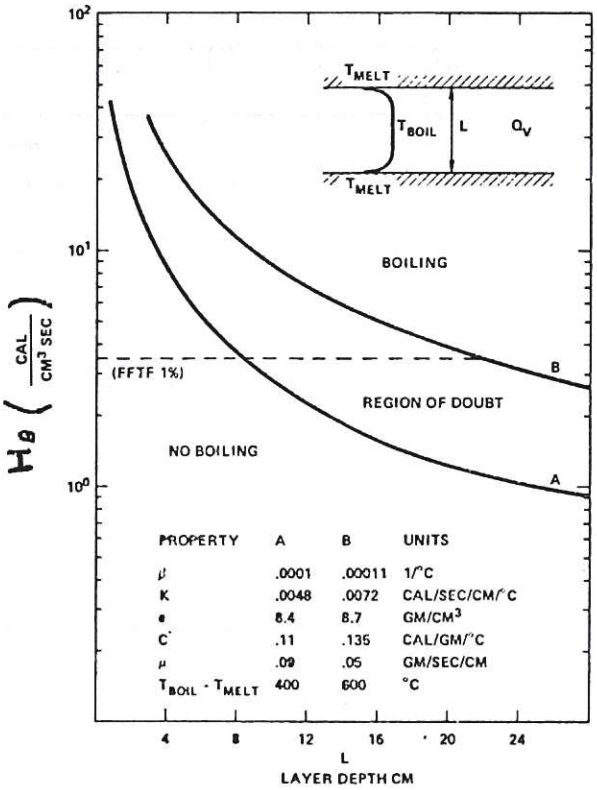

Fig. 4.10 [54]

Boiling and non-boiling regimes in a layer of molten UO_2 with decay heat

For boiling in a container with finite height-to-width ratio, the rising bubbles at high void fractions drive the neutral circulation at enhanced rates. The heat transfer to a sidewall is then a combination of forced and natural convection for a cooled vertical plate. (Chen et al [1976]). Using their model, these authors predict that the solid UO_2 crusts on the sides and top of a boiling UO_2 pool will be very thin (< 1 mm) and may not be able to withstand the mechanical stresses from turbulent fluctuations [29].

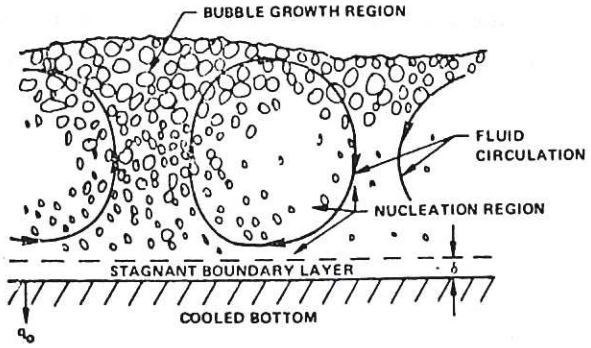

Fig. 4.11 Structure of boiling molten layer [54]

V. PARTICULATE BEDS

After a partial core melt down, a significant fraction of the material involved may be expelled from the core in the form of fine fragments of spectrum of size centred about 100 micron in diameter. Such material will rain down through the sodium and form a bed of particles. This particulate bed will be heat producing because of the decay heat from the fission products. If the rate of heat production is sufficient, the bed may dryout of liquid sodium and may melt down to produce layers of molten core debris. This leads to the following questions. The bed may be considered as a porous medium overlaid by a free liquid layer; if the downward heat transfer from the porous bed to its horizontal support is ignored, under what circumstances will the sodium permeating the bed (i) convect ? (ii) boil ? (iii) dryout ?

V.1 Convection in Porous Media

Thermal convection in a horizontal layer of a porous medium with permeability K is analogous to that in a normal fluid. However the fact that the flow of fluid is now restricted to the pores in the medium means that the viscous term in the Navier-Stokes equation is replaced by the Darcy drag term i.e. $\nu\nabla^2\underline{u}$ is replaced by $-\nu\underline{u}/K$. The Kozeny form for the permeability is $K = c_1 \bar{d}^2 \varepsilon^3/(1-\varepsilon)^2$ where $\bar{d}$ is the mean particle diameter and ε is the mean porosity. c_1 is a constant, found empirically to be $\sim (1/150)$. If a vertical temperature difference is applied across a horizontal porous bed, then as with Benard convection, convection will only occur when the temperature difference exceeds a critical value. A porous Rayleigh number can be defined by $Ra_K = \alpha g \Delta T\, KL/\nu\kappa$ (cf. section §IV.1.1). Clearly $Ra_K = Ra.(K/L^2)$. Convection occurs when $Ra_K > Ra_K^{crit}$. If the bed lies between impermeable plates $Ra_K^{crit} = 4\pi^2$; if a free liquid layer overlies the porous bed $Ra_K^{crit} = 27.1$. Away from the onset of convection the heat transfer is found experimentally to be given by $Nu^* = (1/40)Ra_K$, where $Nu_{cond} = 1$ as for normal Benard convection.

If the porous bed is heated internally, and is placed on an adiabatic bottom, a further modified Rayleigh number can be defined by $Ra_{HK} = \alpha g H L^3 K/(2k\nu\kappa)$ (cf. §IV.1.2) where H is the mean volumetric rate of heat generation. If H' is the heat generation rate in the solid <u>only</u>, $H = H'(1-\varepsilon)$. $T_H \equiv HL^2/2k$ is the temperature difference in the absence of convection. The critical Rayleigh number for the onset of convection in an internally heated porous layer with adiabatic bottom $Ra_{HK}^{crit} = 33$. From arguments analogous to those in §IV.1.2, the heat transfer relationship for internal heat generation would be predicted to be $Nu^* = (Ra_{HK}/40)^{\frac{1}{2}}$. In fact the experimental data can be fitted by the following

correlation (Hardee & Nilson 1977).

$$Nu^* = (Ra_{HK}/43)^{b_5} \qquad (5.1)$$

where $b_5 = 0.573$. This can also be written as $T_H/(T_o - T_1) = (C_2 T_H)^{b_5}$ where C_2 is a constant depending on layer depth and thermophysical properties, T_o and T_1 are temperatures at the bottom and top of the layers.

V.2 Boiling

Boiling will occur in an internally heated porous layer with adiabatic bottom when the temperature T_o at the bottom of the layer reaches the boiling point for the coolant T_B. It does not occur at a unique Rayleigh number; it can occur prior to the onset of single phase convection, or subsequently. In the conduction regime ($Ra_{HK} < Ra_{HK}^{crit}$), the boiling occurs if H is such that $T_H > (T_B - T_1)$. In the convection regime ($Ra_{HK} > Ra_{HK}^{crit}$), boiling occurs when $T_H^{1-b_5} > C_2^{b_5}.(T_B - T_1)$.

V.3 Dryout

If after boiling has started, the heat generation rate is still further increased, a point is reached where the boiling process can no longer carry away all the generated heat and the bed begins to dryout. The modelling of boiling particulate beds is still at rather a tentative stage.

One model is that of Hardee and Nilson (1977). In this model liquid flows downward in one region of the porous bed, and liquid and vapour flow upwards in another region, until near the top of the bed all the liquid is vaporized. Energy balance, continuity, and Darcy's law can be combined to give

$$\frac{HL}{C_L(T_B - T_1) + \mathfrak{L}} = \frac{\rho_L g K}{(\nu_v/\gamma + \nu_L/1-\gamma)}$$

where c_L and ρ_L are specific heat and density of the liquid phase, ν_L and ν_v are the liquid and vapour kinematic viscosities, and $\mathfrak{L}$ is the latent heat of evaporation of the coolant. γ is the vapour void fraction and K is the permeability. Viewing this as an equation for H, as a function of γ, then H takes its maximum value when $dH/d\gamma = 0$ i.e. $\gamma^{-1} = 1 + (\nu_v/\nu_L)^{\frac{1}{2}}$. This leads to the following expression for the dry-out generation rate:-

$$\frac{HL}{C_L(T_B - T_1) + \mathfrak{L}} = \frac{\rho_L g K}{(\nu_v^{\frac{1}{2}} + \nu_L^{\frac{1}{2}})^2}$$

This is a model for a deep bed, in which the top of the bed is at the ambient coolant temperature T_1. Dhir and Catton (1976) have developed a closely related model for a deep bed (see fig. 5.1) in which fluidization occurs in the upper part of the bed, so that in the fixed bed the coolant is at its boiling point. Moreover they take the vapour viscosity to be negligible. The Dhir-Catton form for dry-out of a deep bed is

$$\frac{HL}{\mathcal{J}} = C_3 \frac{\rho_L g k}{\nu_L}$$

where C_3 is a constant to be determined from experiment.

For shallow beds Dhir and Catton (1976) argue that the whole bed fluidizes and that dryout then occurs when instability at the interfaces between down-flowing liquid and upflowing vapour choke the liquid flow.

To measure the dry-out heat flux from a bed of self-heated particles has not been easy mainly because of the difficulty of simulating the decay heat satisfactorily. Early experiments heat the bed of particles from below; subsequently the coolant was joule heated which meant that no heat was being deposited in the vicinity of particles surrounded with vapour. The most satisfactory method so far is to use an induction heater at a frequency which couples strongly with the particles, but not with the coolant. Fig. 5.2 for teflon coated steel particles in water compares the results. For a given bed depth, the dry-out flux is higher for induction heating than for Joule or bottom heating.

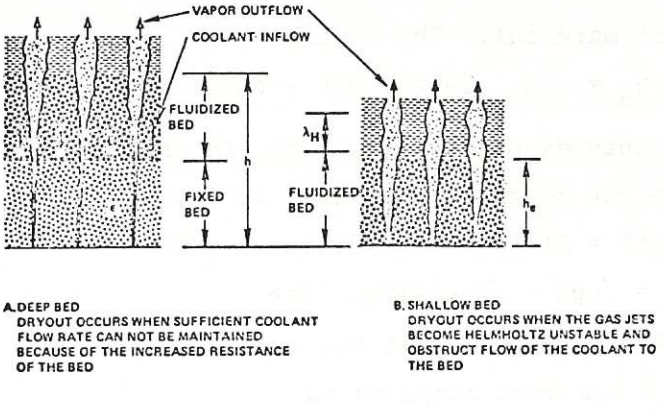

Fig. 5.1 Deep and Shallow Bed Models for Dryout Heat Flux [18]

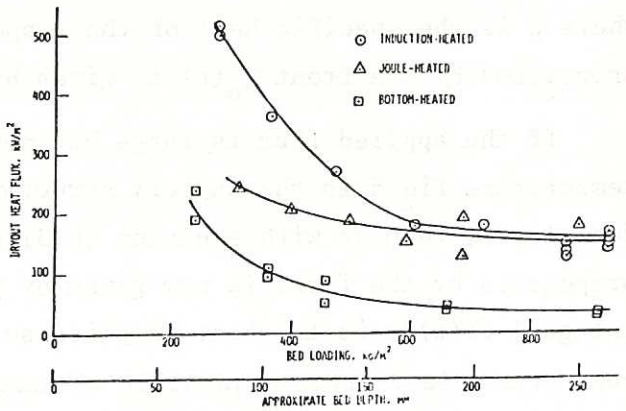

Fig. 5.2 Dryout Heat Fluxes for Teflon-coated Steel Particulate in Water [51]

VI. ADVANCE OF MELTING FRONTS

A molten pool sitting on a support can melt the support structure if the thermal flux is high enough. A melting front will advance into the support. At the front the heat balance is given by

$$F = \rho L u - k \left.\frac{\partial T}{\partial n}\right|_{\text{interface}} \qquad (6.1)$$

where F is the thermal flux incident on the interface, which can be time-dependent, ρ, L, k are the density, latent heat of melting and the thermal conductivity of the support material, $\frac{\partial T}{\partial n}$ is the temperature at the interface in the support material, and u is the velocity at which the front is advancing. Within the support material, the time dependent heat conduction equation is satisfied: $\partial T/\partial t = \kappa \nabla^2 T$, where κ is the thermal diffusivity.

VI.1. Let us consider first of all the advance of a plane interface. If the heat flux is large and constant, then the melting front will propagate into the support material at a velocity u_o. In advance of the front heat is conducted into the support material to raise the temperature to the melting point, and the temperature profile in the frame of reference of the advancing front is unchanging: it has the form

$$T - T_o = (T_m - T_o) \exp(- u_o x/\kappa) \qquad (6.2)$$

where x is the distance from the front T_o is the ambient temperature in the support material and T_m is its melting point. Define $T_m - T_o \equiv \Delta T$. The thermal flux into the support is then $\rho c \Delta T u_o$. Hence from equation (6.1) the velocity u_o is related to the applied thermal flux F by

$$u_o = F/\rho(L + c\Delta T) \qquad (6.3)$$

where c is the specific heat of the support material. The distance propogated by the front $\chi_o(t)$ is given by $\chi_o = u_o t$. Define $\rho(L + c\Delta T) \equiv q$.

If the applied flux is large but now changes slowly with time, so that the temperature field in the support structure can relax continuously to the form (6.2), then as with equation (6.3) $u(t) = F(t)/q$. The distance $\chi(t)$ propogated by the front is now given by $\chi = \int u dt = \int F(t) dt/q$. The integral $\int F(t) dt$ is the heat supplied so far = Q(t). Thus the high heat flux case is simple : after a quantity of heat Q has been supplied to support material which requires q of heat to raise unit volume to the melting point, then the amount of material melted is Q/q.

In considering possible sacrificial materials, one important characteristic is its resistance to melting front advance. The quantity q^{-1} is a good measure of this. Table 6.1 gives the value of q^{-1} for a number

of materials which are worthy of consideration for sacrificial beds because q is large.

The form Q/q for the distance propogated by the melting front after time t is a slight overestimate when the velocity is high. From equation (6.2) the material ahead of the front has been preheated by conduction and its thermal energy above ambient temperature is $\rho c \int_0^\infty (T - T_o)dt$.

i.e. $\frac{k\Delta T}{u}$. Hence $\chi(t) = (Q(t) - \frac{k\Delta T}{u})/q$. While u is large the correcting term is obviously small.

Ranking	Materials	$\frac{1}{q} = \frac{1}{\rho[H_{sf}+C_p(T_m-T_o)]}$ $m^3\ J^{-1}$	T_m = melting point ^oC	ρ = Theoretical density $kg\ m^{-3}$	C_p = Specific Heat $J\ kg^{-1}\ ^oC^{-1}$	H_{sf} = Heat of fusion $J\ kg^{-1}$
1	TaC	$3.90\ 10^{-11}$	3927	$14.50\ 10^3$	355.6	$4.06\ 10^5$
2	BeO	$4.61\ 10^{-11}$	2538	$3.0\ 10^3$	1799	$28.4\ 10^5$
3	NbB_2	$4.92\ 10^{-11}$	2996	$7.12\ 10^3$	795	$5.52\ 10^5$
4	HfO_2	$4.97\ 10^{-11}$	2838	$9.7\ 10^3$	502	$6.99\ 10^5$
5	VC	$5.05\ 10^{-11}$	2732	$5.5\ 10^3$	962	$10.67\ 10^5$
6	TaB_2	$5.19\ 10^{-11}$	3093	$12.6\ 10^3$	414	$2.89\ 10^5$
7	TiN	$5.30\ 10^{-11}$	2926	$5.4\ 10^3$	854	$10.79\ 10^5$
8	MgO	$5.29\ 10^{-11}$	2852	$3.5\ 10^3$	1310	$17.91\ 10^5$
9	TiC	$5.60\ 10^{-11}$	3076	$4.75\ 10^3$	866	$11.84\ 10^5$
10	TiB_2	$5.77\ 10^{-11}$	2870	$4.5\ 10^3$	1130	$7.24\ 10^5$
11	ZrC	$5.81\ 10^{-11}$	3482	$6.6\ 10^3$	544	$7.70\ 10^5$
12	HfB_2	$6.04\ 10^{-11}$	3225	$11.26\ 10^3$	385	$2.68\ 10^5$
13	B_4C	$6.00\ 10^{-11}$	2426	$2.5\ 10^3$	2050	$18.95\ 10^5$
14	NbC	$5.81\ 10^{-11}$	3510	$7.7\ 10^3$	481	$5.94\ 10^5$
15	ZrB_2	$6.38\ 10^{-11}$	3038	$6.1\ 10^3$	711	$4.81\ 10^5$
16	HfC	$6.35\ 10^{-11}$	3926	$12.61\ 10^3$	251	$2.89\ 10^5$
17	ZrN	$6.43\ 10^{-11}$	2982	$7.29\ 10^3$	519	$6.36\ 10^5$
18	BN	$6.47\ 10^{-11}$	2704	$2.26\ 10^3$	1799	$21.5\ 10^5$
19	WC	$6.62\ 10^{-11}$	2760	$15.79\ 10^3$	251	$2.89\ 10^5$
20	ZrO_2	$7.21\ 10^{-11}$	2760	$5.7\ 10^3$	649	$7.07\ 10^5$
21	AlN	$7.38\ 10^{-11}$	2315	$3.30\ 10^3$	1172	$15.1\ 10^5$
22	HfN	$7.49\ 10^{-11}$	3315	$13.9\ 10^3$	209	$2.89\ 10^5$
23	Al_2O_3	$7.64\ 10^{-11}$	2037	$4.0\ 10^3$	1138	$10.7\ 10^5$
24	TaN	$7.59\ 10^{-11}$	3093	$14.4\ 10^3$	209	$2.89\ 10^5$
25	WB_2	$7.73\ 10^{-11}$	2621	$16.0\ 10^3$	251	$1.76\ 10^5$
26	$MoSi_2$	$8.04\ 10^{-11}$	2010	$8.42\ 10^3$	469	$5.82\ 10^5$
27	UO_2	$8.32\ 10^{-11}$	2815	$11.0\ 10^3$	293	$2.97\ 10^5$
28	UC	$8.56\ 10^{-11}$	2371	$13.6\ 10^3$	251	$2.89\ 10^5$
29	ThO_2	$8.11\ 10^{-11}$	3300	$9.95\ 10^3$	293	$3.01\ 10^5$
30	CaO	$8.91\ 10^{-11}$	2593	$3.39\ 10^3$	962	$9.12\ 10^5$
31	Cr_2O_3	$10.5\ 10^{-11}$	2260	$5.20\ 10^3$	795	$1.17\ 10^5$
32	SrO	$10.9\ 10^{-11}$	2454	$4.69\ 10^3$	544	$6.74\ 10^5$
33	SiC	$11.1\ 10^{-11}$	1982	$2.30\ 10^3$	1297	$14.6\ 10^5$

Table 6.1 Materials for a Sacrificial Bed: $T_o = 100^oC$ [26]

If the flux F is negligible, then the molten debris starts to freeze; the melting front becomes in fact a freezing front propogating back into the core debris such that $\chi = -2\lambda\sqrt{\kappa t}$ where λ satisfies $\sqrt{\pi}\lambda\, e^{\lambda^2}(1 + \text{erf}\,\lambda) = c\Delta T/L$. This is the Schwarz solution [11].

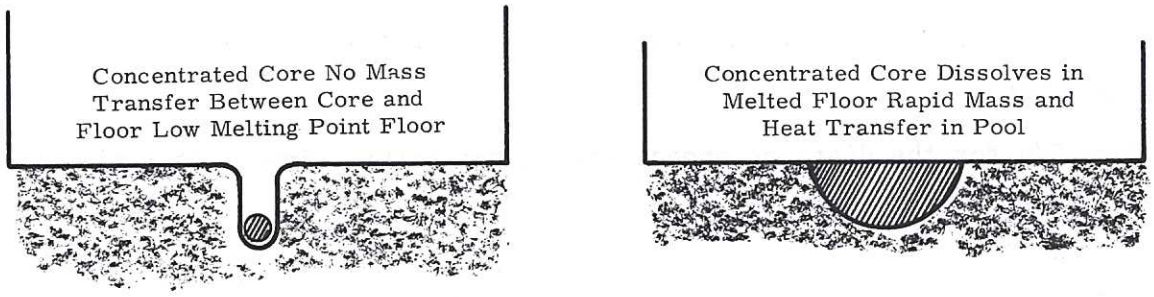

Fig. 6.1 Some Possible Modes of Melting Front Advance [6]

In practice the decay heat F decreases with time (§III); for fuel burn-up of a few hundred days F is roughly $\propto t^{-\frac{1}{4}}$. In these circumstances the plane melting front advances relatively rapidly initially, slows down as F falls, and then as conduction ahead of the front becomes increasingly dominant reaches a maximum position of advance χ_{max}, before solidification begins.

Conduction becomes important when $\kappa t \sim Q_{(t)}^2/\{(c\Delta T)\ \rho q\}$. This implicit equation for t can be used to estimate t_{max} and the corresponding χ_{max}. To follow the progress of the front accurately a numerical solution is required.

The plane layer solution describes the advance of the melt front if the core debris is widely distributed in a layer which can be miscible or immiscible with the support material. It can also be used for a concentrated mass of core debris boring into a low conductivity material, to estimate the maximum depth of penetration on the assumption that a thin skin of material is melted and flows around the core mass, and that lateral conductivity can be neglected. (see fig. 6.1).

VI.2 Cylindrical growth

If the heat flux from the molten core debris in the vertical up and downward directions can be neglected, the pool will grow cylindrically. If R(t) is the pool radius and F is the heat generated per unit depth, then the left hand side of equation (6.1) can be replaced by $F/2\pi R$. Locally near the interface, equation (6.2) still provides an adequate representation of the temperature profile in the solid. The pool radius, for rapid front advance is given by $R^2 = R_2^2 \equiv Q/(\pi q)$. (compared with $\chi = Q/q$ for the plane case). As for the plane case, a correction can be made for the heat content conducted into the solid ahead of the front. This gives $R = R_2 - (k\Delta T/uq)$.

VI.3. Hemispherical growth

If the molten debris forms a hemispherical pool, and the thermal flux through its downward facing surfaces is independent of angle, then the pool grows radially outward. If R(t) is the pool radius (in spherical polars) and F is the heat

generated in the pool (in watts) then the left hand side of equation (6.1) can be replaced by $F/2\pi R^2$. The pool radius, for rapid front advance is now given by $R^3 = R_3^3 \equiv 3Q/(2\pi q)$. With the correction for heat content conducted into the solid ahead of the front, this gives the approximation $R = R_3 - (k\Delta T/uq)$.

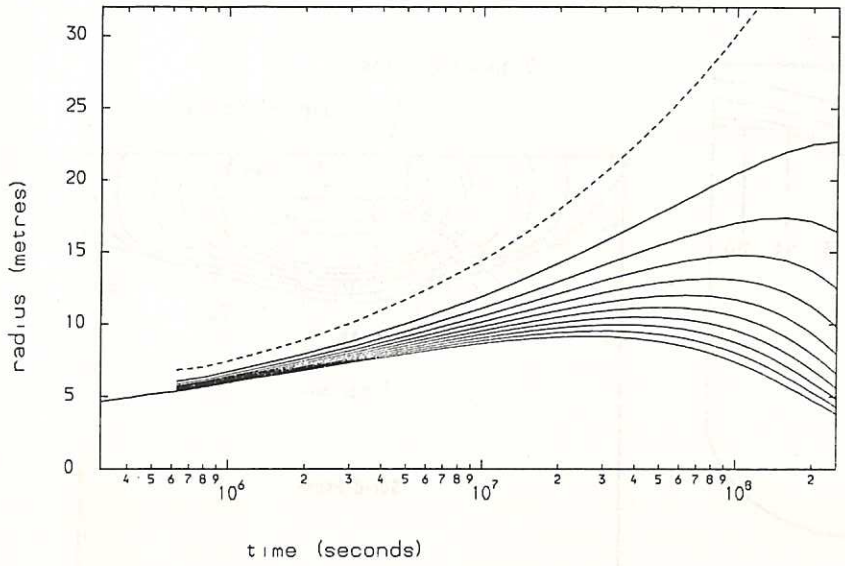

Fig. 6.2
Isotherms for the growth of a hemispherical melt pool for a 672 MWt core [45]

As for the plane case, conduction limits the size of the pool. Fig. 6.2 shows some results obtained with the ISOTHM code[45], integrating the partial differential equations properly. The approximation above gives results for the pool size good to 10% for the debris from a 3GWt reactor.

VI.4. Experiments

Small-scale simulations have been carried out in the laboratory using weak aqueous salt solutions which are Joule heated to provide internal heating, and using water soluble waxes to provide a sacrificial material miscible with the molten pool. The local advance of the melting front is still governed by equation (6.1). However the convection with the molten pool results in the thermal fluxes delivered to the melting front varying with position. Fig. 6.3 shows results obtained by Farhadieh, Baker and Faw (1975). The ratio of densities of pool material ρ_2 to sacrificial material ρ_1 determines the early time behaviour. When ρ_2/ρ_1 is significant the pool penetrates downwards faster than it does sideways. When ρ_2/ρ_1 is ~ 1 the lateral thermal fluxes are larger and the pool grows almost horizontally. Since the density in the molten pool tends to that of the sacrificial material once it has been sufficiently diluted then the later stages of pool growth are always essentially lateral for miscible pools. For immiscible materials where the sacrificial material is lighter, it forms streams of bubbles which rise.

through the pool so that the pool density remains unaltered. The passage of the bubbles through the pool agitates it particularly in the lower boundary layer, thus enhancing the downwards heat transfer. If the bed material were concrete so that quantities of gas were released, this would also result in significant agitation of the pool and changes in the distribution of the thermal flux to the pool boundaries.

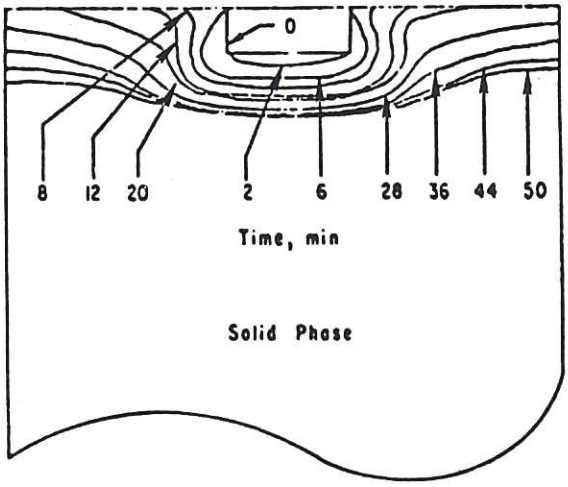

(a) Advancement of Liquid-Solid Interface (100% KI sol'n, 1.5 g/cm^3, 0.9 Cp)

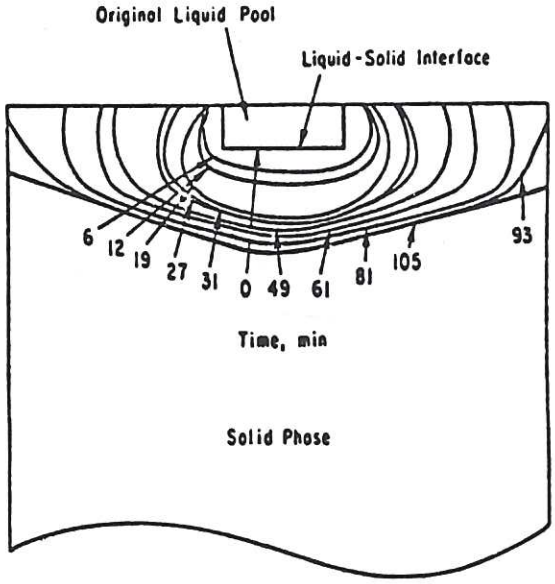

(b) Advancement of Liquid-Solid Interface (20% $ZnBr_2$ - 80% KI sol'n, 1.7 g/cm^3, 2.6 Cp)

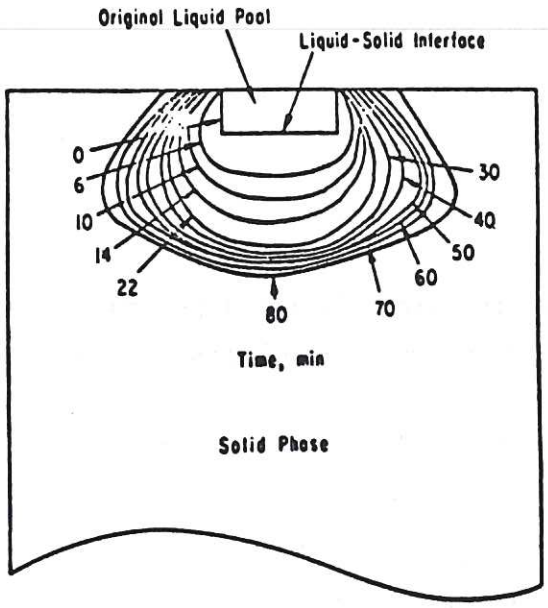

(c) Advancement of Liquid-Solid Interface (80% $ZnBr_2$ - 20% KI sol'n, 2.25 g/cm^3, 9.6 Cp)

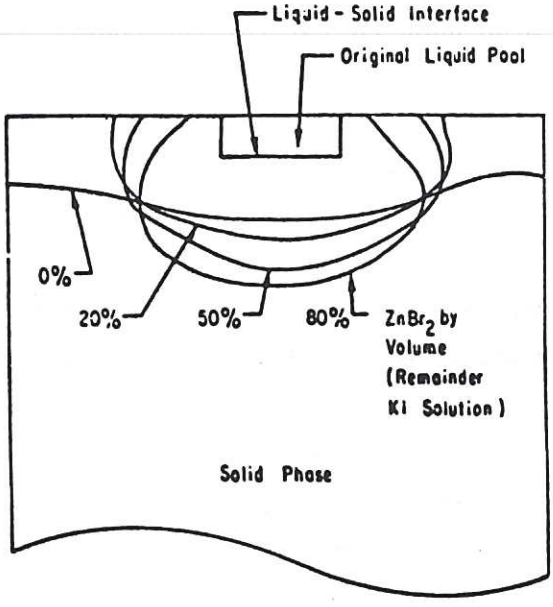

(d) Comparison of Pool Shapes at 50 min.

Fig. 6.3 Advance of Aqueous solutions into water-soluble waxes [19]

VII INTERACTIONS WITH CONCRETE

Significant parts of the overall reactor containment above and below ground level are made of concrete. After a postulated core meltdown the concrete might come into contact with sodium and molten core debris, and be subjected to high temperatures and high thermal fluxes. To assess how good a containment barrier concrete is in these circumstances one needs basic data on

(i) decomposition and melting of concrete by heat fluxes from molten core debris

(ii) chemical interactions between the constituents of concrete and of molten core debris.

(iii) sodium-concrete interactions.

VII.1 Strong heating of concrete can lead to its decomposition and then melting; gases are liberated which may (i) agitate the molten core debris and modify its convection characteristics (see section III) (ii) lead to over-pressurization of the containment and (iii) in certain circumstances lead to hydrogen fires.

If a high thermal flux is incident on the plane face of a slab of concrete, the concrete is gradually eroded. At any stage there are three regions: an outer layer of molten concrete, a layer of decomposed concrete and virgin concrete. As the concrete decomposes, the interfaces bounding these regions propagate inwards at the same rates; the gaseous decomposition products (H_2O, CO_2) counterflow outwards. At Sandia, concrete has been heated in two different experimental rigs: - by a 2 MW Plasmajet and in a Radiant Heat Facility. After subtracting off heat which does not reach the melting interface, Muir (1977) finds that the overall erosion rate is linearly proportional to the net heat flux reaching the melting interface - as one would expect. A flux of 100 W/cm^2 corresponds roughly to 25 cm/hour. The erosion of 1 cm^3 of concrete requires $\sim 10^4$ J. The lack of any systematic dependence on the type of concrete (fig. 7.1) suggests that it is the cement rather than the aggregate which determines the erosion rate.

Depending on the composition of the concrete, up to 30 wt % may be volatilized at high temperatures. Powers (1977) has studied decomposition reactions in two types of concrete (I) based on calcareous aggregate; (II) based on basaltic aggregate. Analyses of small samples of I exposed to linear temperature ramps show three major weight-loss events over the 20 to 1200°C temperature range.

(i) loss of evaporable water in the range 20°C to 200°C. This water is present in the concrete as part of the cement; it constitutes 2 to 3 wt % in I.

(ii) loss of chemically constituted water in the range 200°C to 600°C. This water makes up an additional 2 to 3 wt % of the concrete in the form of hydroxides such as $Ca(OH)_2$ and $Ca_3[Al(OH)_6]_2$ which decompose at these temperatures.

(iii) loss of carbon dioxide in the temperature range 650°C to 1200°C Decarboxylation of calcium carbonate in the aggregate and cementitious particles of I may involve more than 22 wt % of the cement. In II however this loss is < 2 wt %.

The kinetics of these weight-loss events may be empirically described by activated first-order rate laws of the form

$$d\alpha_i/dt = (1-\alpha_i)\exp(a_i \pm \Delta a_i)\exp[(-b_i \pm \Delta b_i)/T]$$

where least squares fitting of experimental data gives the values in table 7.1. T is the absolute temperature, t is the time in minutes and α_1, α_2, α_3 are the weight fractions of evaporable water, chemically constituted water and carbon dioxide lost from the concrete respectively.

Table 7.1 Rate Constants for Concrete Decomposition [47]

	a_i	Δa_i	b_i	Δb_i	
i=1	14.07	5.97	5557	867	evaporable water
i=2	28.31	1.43	20560	556	chemically constituted water
i=3	16.8	11.0	19362	6816	carbon dioxide

Melting for both kinds of concrete occurs at 1100 ± 20°C; its onset is associated with the cementitious material. Complete liquefaction depends on aggregate type and occurs at 1400 ± 50°C. The latent heat associated with concrete melting is 100 ± 30 cal/g and is small compared with the calorific input required to raise the concrete to its liquidus temperature.

The volume of gas evolved is considerable and its rapid and vigorous production will violently agitate the overlying melt as Powers (1977) found when he dropped 200 kg of mild steel at 1700°C into concrete crucibles. In these experiments the gases were reduced on passage through the melt to H_2 and CO, which readily ignite in air.

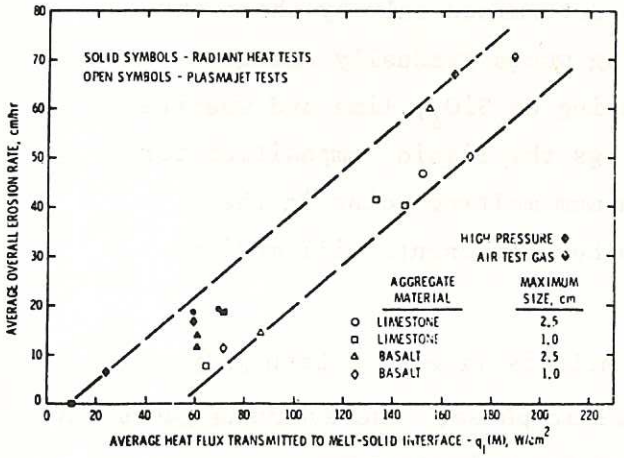

Fig. 7.1 Overall Erosion Rate vs net heat flux to concrete melting front [39]

VII.2 Chemical Interactions

Concrete and molten core debris both consist of a number of different components. The mutual solubilities of the concrete constituents with those of the core debris, the formation of complex slags and the time scales on which the reactions occur will effect the hydrodynamics of the molten debris pool, and hence its growth and shape. An informed view of the magnitude of the task of incorporating these effects properly can be gained from reading Powers' review, chapter 4 in SAND74. (also chapter 9).

Typical aggregate materials used in the manufacture of concrete are limestone, basalt and silicate rock. The aggregate material is mixed with Portland cement and water in the weight ratios 31:5:2 approximately. The main constituents of the typical resulting concretes are shown in table 7.2.

Table 7.2 Main Constituents of Concrete by weight percent

with limestone aggregate	with basaltic aggregate	with siliceous aggregate
CaO (41)	SiO_2 (45)	SiO_2 (57)
CO_2 (29)	CaO (17)	Al_2O_3 (13)
SiO_2 (14)	Al_2O_3 (13)	CaO (13)
H_2O (7)	"FeO" (9)	H_2O (7)
	H_2O (7)	

Also MgO, Na_2O and K_2O_3 are present at the few percent level. The main constituents of core debris are UO_2 and iron in roughly equal quantities.

After complete concrete-melt interaction has occurred (if it does), with H_2O and CO_2 oxiding the iron, the resulting slag is composed mainly of FeO, CaO and SiO_2 with UO_2 concentration in the 4-7 mole percentage range. In the ternary phase diagram for the three main components, the limestone-generated slag is in the Ca_2SiO_4 region, the basalt slag is in the wollastonite region, and the silica rock slag in the tridymite

region. If the solidification process were determined only by these three components, then the limestone-generated slag would gradually change towards the eutectic composition, precipitating Ca_2SiO_4, lime and wustite, and freeze at 1283°C. For the other two slags the liquid composition for both would gradually change towards the minimum melting point in the wollastonite region at about 1093°C. The other components will modify these conclusions to some extent.

In the melt-down process however, the melt is likely to be highly inhomogeneous with an oxide phase and a metallic phase; the evolving gases may not have time or sufficient access to oxidize the molten iron.

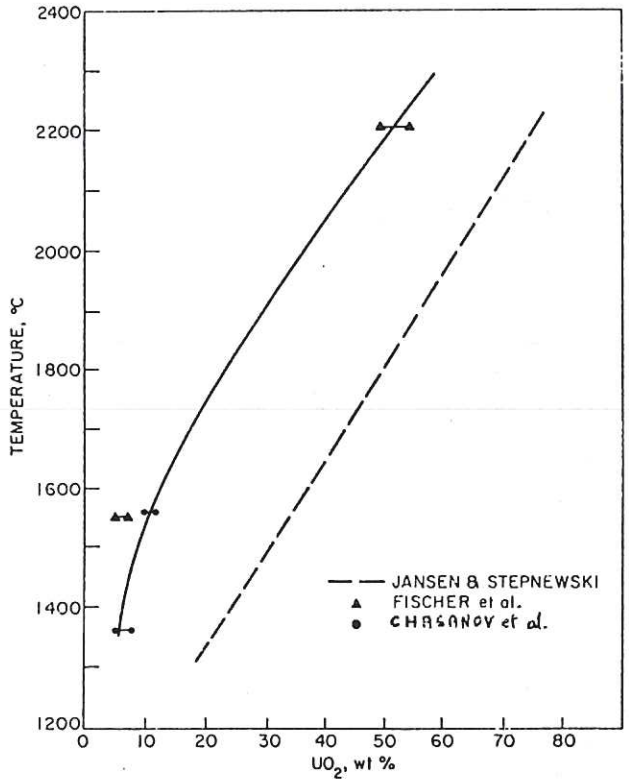

Fig. 7.2 Melting point of UO_2 solution in Columbia River Basalt [13]

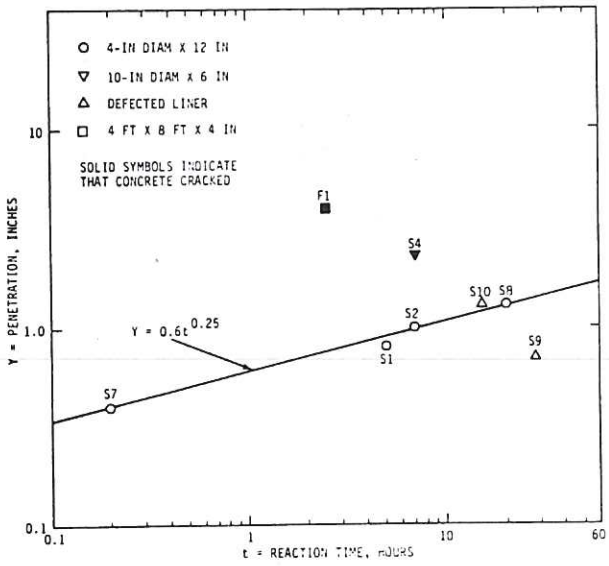

Fig. 7.3 Penetration of sodium into concrete [31]

Another question concerns the solubility of UO_2 in concrete materials. Experiments have been carried out at ANL with uranium dioxide microspheres and molten Columbia River basalt. These indicate that the solubility of UO_2 in basalt is 6 wt % at 1350°C, 10 wt % at 1560°C and 50 wt % at 2200°C. see figure 7.2 (from Chasanov et al 1974).

VII.3 Sodium-concrete interactions The presence of sodium provides two additional complications. First potentially it can react exothermally with both the water content and some of the solid constituents of concrete, thus adding to the burden of heat to be removed. Secondly appreciable quantities of hydrogen can be generated by sodium-water reactions; this can contribute to pressurization of the containment, or burn in an oxygen rich atmosphere (> 5% O_2). Brief details of experiments in which sodium has been spilt onto concrete are given in a review by Hilliard (1975).

The important reactions which can occur between sodium and various constituents are listed in table 7.3. These reactions can be divided into two groups. The first three reactions concern the reaction with water or hydrogen, which are mobile and thus can occur outside the concrete boundary. The remaining reactions concern solid reactants and thus must take place within the concrete matrix with sodium being the mobile reactant. The reactions producing sodium silicate are merely representative of a wide number of reactions producing $Na_2O.(SiO_2)$. Heats of reaction for conventional (SiO_2, basalt) concrete, high density concrete, portland cement, and SiO_2 have been calculated from standard thermophysical properties by Hilliard and also deduced from a differential thermal analysis of appropriate samples. The results are given in table 7.4. Reactions with sodium become significant above $\sim 630^{o}C$ for standard concrete and $\sim 460^{o}C$ for magnetite concrete.

Small-scale HEDL tests showed that the rate of penetration of sodium into concrete falls with time, indicating that the solid reaction products which form a compact layer at the surface are limiting the rate of reaction. An empirical equation for the reaction rate is $R = (A/80)t^{-\alpha}$ where $\alpha = 0.75$, R is the reaction rate in ft^3/hr, A is the surface area in ft^2 and t is the time in hours. The penetration with time for the HEDL tests is given in fig.7.3. However if the concrete is cracked by thermal or mechanical stresses then the reaction can propogate much more rapidly.

We have already considered the water released by heating concrete without sodium; with sodium present the fraction of water which reacts with sodium to form hydrogen depends on their mutual accessibility. If the water is released from the concrete directly into the containment atmosphere above the sodium pool, then some water will condense on superstructural surfaces and some will be swept out by convection into the outer parts of the containment; the formation of sodium hydroxide on the surface of the sodium pool can also inhibit sodium-water reactions. In one HEDL experiment under these circumstances only 5 kg of water reacted to form H_2 out of 50 kg of water released. If the water is

released directly into the sodium pool, then there is essentially 100% conversion to H_2 .

It should be remarked that while a steel liner, if unflawed, can separate sodium from concrete, it cannot inhibit the evolution of H_2O and CO_2 which are produced by heat alone. Thus if strong pressures ($\sim$ 10 bars) are not to be built up behind such a liner, venting routes are needed within the concrete. Dayan and Gluekler (1977) estimate that vent holes 4 m apart are sufficient to allow the gases to escape with pressurization of the liner of less than 0.1 bar.

Table 7.3 Sodium-Concrete Reaction Equations (from [31])

			$-\Delta H^{298}$ Btu/lb Na
(1)	$2\ Na_{(1)} + H_2O_{(g)}$	$\rightarrow\ Na_2O_{(c)} + H_{2(g)}$	1680
(2)	$Na_{(1)} + H_2O_{(g)}$	$\rightarrow\ NaOH_{(c)} + 1/2\ H_{2(g)}$	3530
(3)	$Na_{(1)} + 1/2\ H_{2(g)}$	$\rightarrow\ NaH_{(c)}$	1100
(4)	$4\ Na_{(1)} + 3\ SiO_{2(c)}$	$\rightarrow\ 2\ Na_2SiO_{3(c)} + 3\ Si_{(c)}$	2220
(5)	$6\ Na_{(1)} + Fe_2O_{3(c)}$	$\rightarrow\ 3\ Na_2O_{(c)} + 2\ Fe_{(c)}$	1350
(6)	$2\ Na_{(1)} + FeO_{(c)}$	$\rightarrow\ Na_2O_{(c)} + Fe_{(c)}$	1420
(7)	$Na_2O_{(c)} + SiO_{2(c)}$	$\rightarrow\ Na_2\ SiO_{3(c)}$	2630

Table 7.4 Heats of Reaction [31]

	Calculated*	Westinghouse Research Lab	HEDL TME 74-36
Magnetite Concrete	1050	900 $\pm$ 270	700 $\pm$ 350
Conventional Concrete	770	240 $\pm$ 240	-
Sand	1130	820 $\pm$ 820	-
Portland Cement	98	50 $\pm$ 50	-

*Calculated from Standard Thermochemical Properties. Expressed as Btu per lb concrete.

VIII. CORE CATCHER DEVICES

The primary object of a core catcher is to bring molten core debris to rest in a coolable configuration without the escape of radioactive fission products. A core catcher can be either (a) in-vessel, i.e. within the primary tank or (b) ex-vessel, i.e. the containment envelope is enlarged to include an ex-vessel device.

The types of catcher can be considered under the headings of (i) sacrificial beds (ii) crucible concepts (iii) tray concepts. Table 8.1 lists the main advantages and disadvantages of each of these concepts. Fig. 8.1 illustrates schematically, some possible realizations of these concepts for a pool type LMFBR. The devices for a loop type reactor would be similar for the ex-vessel concepts.

An in-vessel system has the advantage that the containment envelope is not enlarged. Moreover there is already present a large quantity of sodium, which is adequate for heat rejection of the decay heat after a normal reactor trip. An ex-vessel system has the advantage that since it is not in contact with high temperature sodium under normal operation, the choice of potential materials is widened; for example, neutron poisons can be incorporated into an ex-vessel device.

Table 8.1 Types of Core Catcher [26]

Design Concept	Features	Advantages	Disadvantages	Uncertainties
Sacrificial Bed (UO_2, ThO_2, MgO, Graphite, etc.)	Large volume cylindrical bed with smaller size containment hole for debris at upper surface Ex-Vessel system	Potentially passive system	High cost if UO_2 or ThO_2 are used Large cavity size required High upward heat flux	Mixing Distribution of heat fluxes End of melting process
Crucible Concepts	Flat stainless steel crucible with UO_2 graphite, or Cu coating at inner surface In- or Ex-vessel system	Defined containment of molten core debris Limited upward heat flux	Active cooling system required	Effect of initial transient conditions on structural stability Dispersion of debris and debris size
Tray Concepts	Multi-tray concept with small volume containers submerged in sodium Preferably in-vessel system	Low temperature system Dispersal of fragmented core debris	Active cooling system required for sodium pool Uncertain core debris dispersal	Distribution of fragmented particles in trays (mass flow) Structural feasibility

It is now clear that molten core debris can be satisfactorily cooled; what is not clear is what is the optimum choice of device, which depends on the importance that one attaches to passive versus active cooling systems, the probabilities of availability of active systems, and the desirability of cooling the molten debris rapidly or of allowing it to cool slowly once it has attained a stable configuration.

More detailed discussion of various concepts can be found in Gluekler (1975, 1976), Peckover (1973, 1974) in the PAHR information exchange proceedings [2] and in the Sandia Core Meltdown Review (chapter)12 [6].

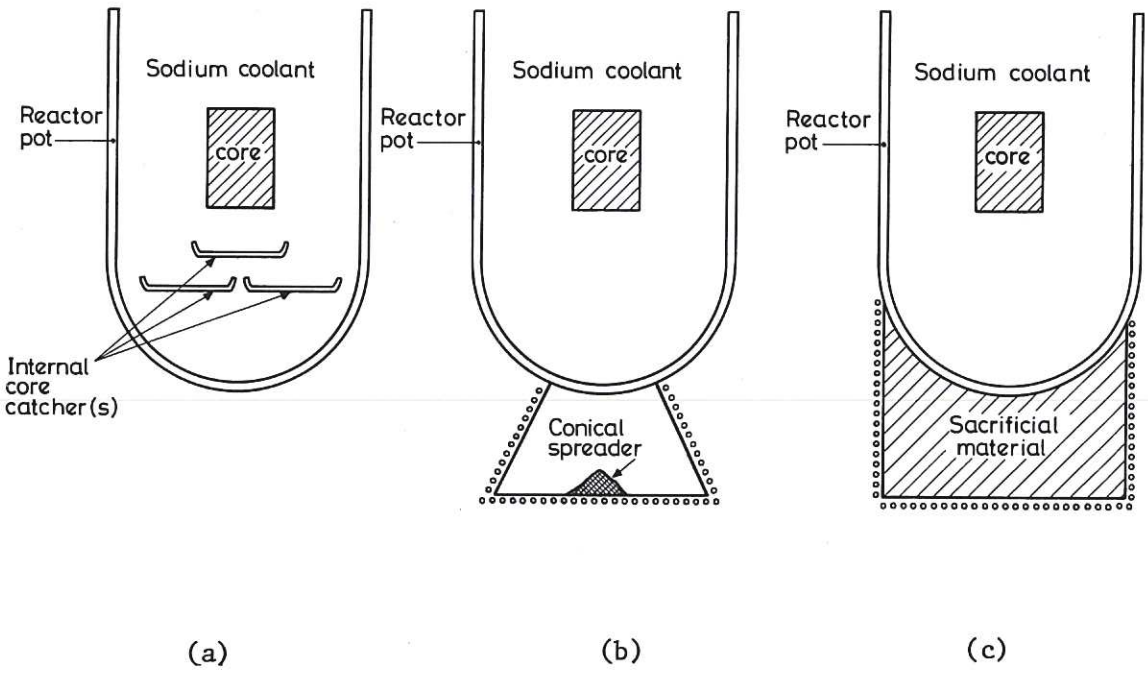

Fig. 8.1 (a) Internal Catcher tray, or possibly an array of trays, possibly with forced auxiliary cooling.

(b) Crucible with conical spreader, and auxiliary cooling; possibly with a thick liner.

(c) Cylindrical Sacrificial bed; possibly with auxiliary cooling.

IX RECRITICALITY

Most of the neutrons produced in a fast reactor are used to maintain the chain reaction : however some neutrons are absorbed by sodium and by the steel clad; some neutrons escape and are used by the breeder blankets. After a core meltdown the configuration is no longer well defined and it is important in designing any long term retention device for core debris to be clear under what circumstances, if any, secondary criticality might occur. In practice the core debris will be some mixture of UO_2/PuO_2 fuel, and steel from clad, subassembly wrappers and various support structures. If a liner were used on a retention device e.g. of depleted UO_2, that material must also be considered.

To obtain a general insight into the minimum quantities of fuel required for secondary criticality, we consider now a few simple but representative geometries, using as fuel a mixture of UO_2/PuO_2 with a Pu enrichment of 27%, and a theoretical density of 9.7 g/cc. The results below are from Pena, Kussmaul, Froehlich (1975) and were obtained using a transport (S_8) theory criticality code.

For a sphere surrounded by (a) sodium or (b) depleted UO_2 or (c) a vacuum the minimum size and mass is given in table 9.1.

Table 9.1 Criticality Calculations for Mixed-Oxide Fuel Spheres (from [46])

PuO_2/UO_2 Sphere Surrounded By	Critical Radius of PuO_2/UO_2 Sphere (cm)	Critical Volume of PuO_2/UO_2 Sphere (L)	Critical Mass of PuO_2/UO_2 Sphere (kg)
Na	21.3	40.6	393.8
Depleted UO_2	17.6	22.9	222.3
Vacuum	23.9	57.25	555.4

The smallest diameter is $\sim$ 35 cm when the sphere is surrounded by depleted UO_2. When surrounded by sodium, the mass required is nearly twice as great. In vacuo the mass required is 2.5 times that required when depleted UO_2 is used. A current fast reactor core can contain 4-10 tonnes of fuel.

In other geometries, a vertical cylinder of oxide fuel surrounded by Na or in vacuo needs a diameter in excess of 30 cm to be able to become critical. If the fuel is in the form of a flat cylinder of radius 100 cm, resting on steel or depleted UO_2 and surrounded by sodium, then it is

subcritical if the cylinder height is less than 14 cm. If 4 tonnes of fuel is in the form of a hollow annulus resting on depleted UO_2 and otherwise surrounded by sodium, then if the inner diameter is less than 180 cm, the system is subcritical.

Steel may also be mixed in with the fuel. Considerable voidage may also be present. Fig. 9.1 shows how the critical radius of a sphere varies with either UO_2 or Na as surround when

(a) steel of volume fraction 24% is included i.e. the steel of the clad

(b) steel of volume fraction 40% is included i.e. all the steel in the core.

For a porosity of 50%, then to achieve criticality 1700 kg of oxide fuel is needed if clad steel is included, and 2300 kg of oxide fuel is needed if a mean core steel fraction is included.

On the basis of these calculations, secondary recriticality will not occur for a small meltdown, but cannot be ruled out if a significant fraction of the core melted. One of the advantages of an ex-vessel device is that a neutron poison can easily be incorporated in it.

Fig. 9.1 Critical radius vs porosity for a PuO_2/UO_2/steel sphere surrounded by Na or depleted UO_2 (from [46])

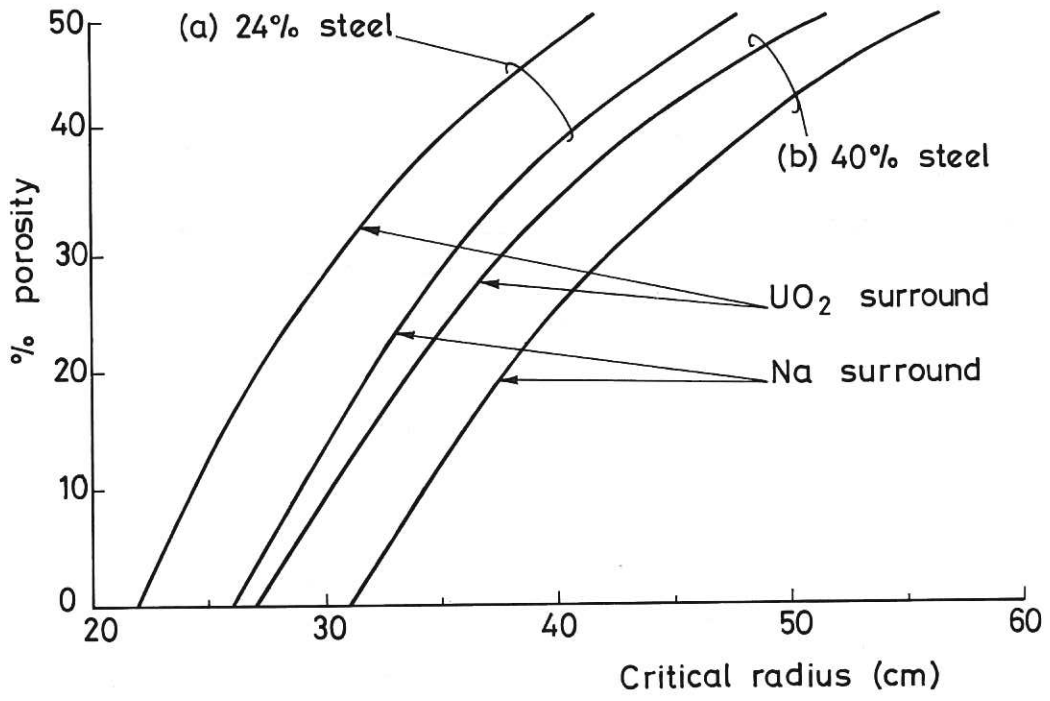

X. MATERIAL PROPERTIES

Modelling the fluid dynamics and heat transfer of multiphase systems is sufficiently complex that it is important that uncertainties introduced from inadequate knowledge of material properties should be minimized. During the past ten years there has been a substantial increase in the data available for the thermophysical properties of materials relevant to core meltdown studies, especially at high temperatures. The volume of data is now such that it is impossible to summarize it in a brief section of a review like this. Nevertheless it is valuable to be able to find material properties data quickly; in the following paragraphs the main data compendia are indicated and shortcomings in the data pointed out.

The following properties are needed for PAHR studies in both the solid and liquid states:- (i) melting temperature (ii) latent heat of fusion (iii) boiling point (iv) latent heat of vaporization (v) specific heat (vi) thermal diffusivity (vii) thermal conductivity (viii) thermal expansion coefficient (ix) density (x) viscosity (xi) surface tension (xii) thermal emissivity. In particular their dependence on temperature is required. In other reactor safety studies (for example whole core accident analysis or fuel coolant interaction modelling) the properties of the vapour state are required as are the variations with pressure. We concentrate here on unpressurized systems.

The materials of primary interest are (i) sodium (ii) UO_2 (iii) oxide fuel (iv) stainless steels. Other relevant materials are concrete, and candidate materials for sacrificial beds.

(i) Sodium

Since the melting point of sodium is 98°C, the properties of solid sodium are not of much interest in this context. For liquid sodium, all the properties listed above except the thermal emissivity are given over the liquid temperature range in Golden and Tokar (1967). Updated values are given in the Argonne compilation of properties for LMFBR safety analysis (1976) [hereafter called ANL76]. Chasanov et al (1973) provides a convenient summary of the main properties. See also the ANL report ANL-8120. [13].

(ii) Stainless Steel

The compilation ANL76 provides recommended values for all the properties listed above except the surface tension and thermal emissivity. The basis for the recommendations is expanded in Kim (1975). For viscosity it recommends the use of the viscosity of molten iron, as does the Sandia review SAND74, based in this case mainly on Russian experimental work. The emissivity of various stainless steels is also given in SAND74 for both solid and molten steels.

(iii) UO_2

The compilation ANL76 again provides recommended values; SAND74 reviews the experimental data available. No value is available for the thermal conductivity of liquid UO_2 or for the thermal emittance of liquid UO_2. Conflicting values are reported for the viscosity of UO_2. viz. $\sim$ 40 cp by Bates, 7-9 cp by Tsai and Olander, $\sim$ 4 cp by Woodley. The lower values are more recent. As one might expect the data for UO_2 at high temperatures is still rather uncertain, and not of the "reference" quality one can associate with sodium. The thermal conductivity of solid UO_2 is reasonably well established. The boiling point of UO_2 is still uncertain to 5% - ANL76 quotes 3760 K $\pm$ 200 K. [see also SAND74 and Chasanov et al (1973)] .

(iv) Mixed Oxide

The compilation ANL76 provides the density, the thermal conductivity, the specific heat, and the thermal expansion coefficient for mixed oxide fuel (Pu $\sim$ 20-25%). For the emittance, surface tension, and viscosity, as yet unmeasured, it recommends the use of UO_2 values. For solid mixed oxide fuel Bard et al (1974) have summarized in a HEDL report available experimental data for specific heat, thermal expansion coefficient and thermal conductivity. Another useful source of data on solid mixed oxides is Olander's text (1976) on fuel elements which has a companion volume of worked examples.

(v) Concrete and Basalt

Data on concrete and basalt at elevated temperatures is still rather sparse. See SAND74 for some references.

(vi) Mixtures

Very little thermophysical data exists for various coria, i.e. for molten core debris mixed in specific fractions, and for coria mixed with concrete, basalt and other sacrificial bed materials. Work is in progress in a number of laboratories, including JRC Ispra, to rectify this situation.

In summary, reproducible material properties at high temperatures and for mixtures of materials are difficult to obtain; this is the area where PAHR needs material properties and although the data base is much sounder than it was much more is required and there is a continuing need for experiments in different laboratories to provide cross-checks and increased confidence.

CONCLUSIONS

This is intended to be an introductory survey. Each of the topics mentioned needs to be studied in much greater depth. The behaviour of individual elements, e.g. particulate beds, molten pools, concrete, has been touched on; their possible mutual interactions and transitions are still rather ill defined, and more analysis is required.

REFERENCES

A. General References and Recent Conferences

[1] Proceedings of the Fast Reactor Safety Meeting, BEVERLY HILLS, April 1974. USERDA report CONF-740401.

[2] Coats R L (Editor) The Second Annual Post-Accident Heat Removal Information Exchange ALBUQUERQUE, November 1975. Sandia report SAND76-9008.

[3] Proceedings of the ANS-ENS international meeting on Fast Reactor Safety and Related Physics CHICAGO, October 1976 USERDA report CONF-761001.

[4] Transactions of the American Nuclear Society (1976) volume 23. Record of the Toronto meeting June 1976.

[5] Transactions of the American Nuclear Society (1977) volume 26. Record of New York meeting June 1977.

[6] Core Meltdown Experimental Review (1975) Sandia Report SAND74-0382 [called SAND 74 in the text].

[7] Leibowitz L (1976) Properties for LMFBR Safety Analysis Argonne Report ANL-CEN-RSD-76-1 and supplement 1 [called ANL76 in the text].

[8] Thompson T J and Beckerley J G (1973) The Technology of Nuclear Reactor Safety, Volume 2: Reactor Materials and Engineering. 820 pp. M.I.T. Press.

B. Additional Material

[9] Baker L Jr., Faw R E and Kulacki F A (1976) Post Accident Heat Removal - Part I: Heat Transfer Within an Internally Heated, non boiling Layer. Nucl. Sci. and Eng. 61, 222-230.

[10] Bard F E, Gneiting B C and Cox C M (1974) Thermoelastic Material Properties for U/Pu mixed oxides. Hanford Report HEDL-TME-74-12.

[11] Carslaw H S and Jaeger J C (1959) Conduction of heat in solids 2nd Edition. Oxford University Press.

[12] Chasanov M G, Leibowitz L and Gabelnick S D (1973) High temperature physical properties of fast reactor materials J. Nucl. Materials 49, 129-135.

[13] Chasanov M G et al (1974) Reactor Safety and Physical Property Studies - Annual Report July 1973 - June 1974. Argonne Report ANL-8120.

[14] Chen J C, Gustavson W R, Kazimi M S (1976) Heat Transfer from a volume-heated boiling pool. Ref. [4], above, p.367.

[15] Chu T Y and Goldstein R J (1973) Turbulent Convection in a Horizontal Layer J. Fluid Mech. 60, 141.

[16] Dayan A and Gluekler E L (1977) Heat and Mass Transfer behind a heated reactor cell liner Ref. [5] above, p.401.

[17] Dearsdorff J W (1970) Convective velocity and temperature scales for the unstable planetary boundary layer and for Rayleigh convection. J. Atmos. Sci. 27, 1211-13.

[18] Dhir V K and Catton I (1976) Prediction of Dryout Heat Fluxes in beds of volumetrically heated particles Ref. [3] above, p.2026.

[19] Farhadieh R, Baker L Jr. and Faw R E (1975) Studies of Pool Growth with Simulant Materials Ref. [2] p.271.

[20] Fiedler H E and Wille R (1970) Turbulente Freie Konvection in Einer Horizontalen Flussigheitsschict mit Volumen Warmequelle. Proc. 4th Int. Heat. Transf. Conf. paper NC4.

[21] Fischer J, Schilb J D and Chasanov M G (1973) Investigation of the Distribution of fission products among molten fuel and reactor phases. J. Nucl. Materials 48, 233-240.

[22] Fitzjarrald D E (1975) An experimental study of turbulent convection in air J. Fluid Mech. 73, 693.

[23] Gabor J D, Baker L Jr. and Cassulo J C (1975) Heat Removal from Heat Generating Pools. Ref. [2] above p.133.

[24] Garon A M and Goldstein R J (1973) Velocity and Heat Transfer Measurements in thermal convection. Phys. Fluids 16, 1818-1825.

[25] Gershuni G Z and Zhukhovitsky E M (1976) Convective Stability of incompressible fluids I.P.S.T. Jerusalem

[26] Gluekler E L (1975) Status of Post-Accident Core Retention Concepts and Models. General Electric Report GEAP-14048.

[27] Gluekler E L (1976) Ex-Vessel Core Retention Concept for Early Sized LMFBR General Electric Report GEAP-14121.

[28] Golden G H and Tokar J V (1967) Thermophysical Properties of Sodium Argonne Report ANL-7323.

[29] Gustavson W R, Kazimi M S and Chen J C (1975) Heat Transfer and fluid dynamics in a volume heated boiling pool. Ref. [3] above, p.2066ff.

[30] Hardee H C and Nilson R H (1977) Natural Convection in Porous Media with Heat Generation. Nucl. Sci. and Eng. 63, 119-132.

[31] Hilliard R K (1975) Sodium-Concrete reactions, Liner Response, and Sodium Fire Extinguishment Ref. [2] above, p.297.

[32] Jahn M and Reineke H H (1974) Free Convection heat transfer with internal heat sources. Proc. 5th Int. Heat. Trans. Conf. Tokyo.

[33] Joseph D D (1976) Stability of Fluid Motions Vol. II, Springer-Verlag.

[34] Kim C S (1975) Thermophysical Properties of Stainless Steels Argonne Report ANL-75-55.

[35] Kulacki F A (1971) Thermal Convection in a Horizontal Fluid Layer with Uniform Volumetric Energy Sources, Ph.D. Thesis, Minnesota.

[36] Kulacki F A and Emara A A (1975) High Rayleigh Number Convection in Enclosed Fluid Layers with Internal Heat Sources US-NRC report NUREG-75/065.

[37] Kulacki F A and Goldstein R J (1972) Thermal convection in a horizontal fluid layer with uniform volumetric energy sources. J. Fluid Mech. 55, 271.

[38] Kulacki F A and Nagle M E (1975) Natural Convection in a Horizontal Fluid Layer with Volumetric Heat Sources. J. Heat. Trans. 97C, 204.

[39] Muir J F (1977) Response of Concrete to High Heat Fluxes Ref. [5] above, p.399.

[40] Olander D R (1976) Fundamental Aspects of Nuclear Reactor Fuel Elements 612pp USERDA report TID-26711.

[41] Peckover R S (1972) The Effect of Convection on Heat Transfer with Heat Sources II UKAEA Report CLM-M91.

[42] Peckover R S (1973) The Use of Core Catchers in Fast Reactors. Proc. Fast Reactor Safety Conf., p.830ff Karlsruhe Oct. 1973.

[43] Peckover R S (1974) The Thermal Containment of Reactor Core Material after Shutdown Ref. [1] above, p.802.

[44] Peckover R S and Hutchinson I H (1974) Convective Rolls driven by Internal Heat Sources, Phys. Fluids 17, 1369.

[45] Peckover R S, Turland B D and Whipple R T P (1977) On the Growth of Melting Pools in Sacrificial Materials. The Third Annual Post-Accident Heat Removal Information Exchange Chicago 1977.

[46] Pena J, Kussmaul G and Froehlich R (1975) Criticality Calculations for Hot UO_2/PuO_2/Steel mixtures with variable steel content and porosity. Ref. [2] above, p.43.

[47] Powers D A (1977) Empirical Models for the thermal decomposition of concrete and Large-scale melt/concrete interaction tests Ref. [5] above p.400.

[48] Ralph J C, McGreevy R and Peckover R S (1976) Experiments in Turbulent thermal convection driven by internal heat sources Proc. Int. Conference on 'Turbulent Buoyant Convection' Dubrovnik September 1976.

[49] Ralph J C and Roberts D N (1974) Free Convection Heat Transfer Measurements in Horizontal Liquid Layers with Internal Heat Generation UKAEA Report AERE-R7841.

[50] Reineke H H (1975) Thermohydrodynamic Behaviour and Heat Transfer in the Molten Core. Ref. [2]above, p.181.

[51] Sowa E S, Gabor J D, Baker L Jr., Pavlik J R, Cassulo JC and Holloway W (1976) Studies of the formation and cooling of particulate fuel debris beds in sodium. Ref. [3] above p.2036ff.

[52] Sparrow E M, Goldstein R J and Jonsson V K (1963) Thermal Instability in a horizontal layer: effect of boundary conditions and non-linear temperature profile. J. Fluid Mech. 18, 513.

[53] Stein R P, Hesson, J C and Gunther W H (1974) Studies of Heat Removal from Heat Generating Boiling Pools. Ref. [1] above, p.865.

[54] Suo-Anttila A J, Catton I and Erdmann R C (1974) Boiling Heat Transfer from Molten Fuel Layers Ref. [1] above, p.845.

[55] Suo-Anttila A J, and Catton I (1975) Thermal Convection Experiments with internal heating. Ref. [2] above, p.161

[56] Holtbecker H et al. (1977) Joint Research Centre Ispra document EUR/C-IS/1/77-e.

Acknowledgements

This work has been carried out with the support of the Safety and Reliability Directorate of the UKAEA at Culcheth.